NAVAL POSTGRADUATE SCHOOL

MONTEREY, CALIFORNIA

THESIS

ELECTROMIGRATION RELATED EFFECTS AT METAL-METAL INTERFACES: APPLICATION TO RAILGUNS

by

William Bryant Cleveland Jr.

March 2007

Thesis Advisor: Indranath Dutta

Approved for public release; distribution is unlimited

THIS PAGE INTENTIONALLY LEFT BLANK

REPORT DOCUMENTATION PAGE			Form Approved OMB No. 0704-0188
Public reporting burden for this collection of information is estimated to average 1 hour per response, including the time for reviewing instruction, searching existing data sources, gathering and maintaining the data needed, and completing and reviewing the collection of information. Send comments regarding this burden estimate or any other aspect of this collection of information, including suggestions for reducing this burden, to Washington headquarters Services, Directorate for Information Operations and Reports, 1215 Jefferson Davis Highway, Suite 1204, Arlington, VA 22202-4302, and to the Office of Management and Budget, Paperwork Reduction Project (0704-0188) Washington DC 20503.			
1. AGENCY USE ONLY *(Leave blank)*	**2. REPORT DATE** March 2007	**3. REPORT TYPE AND DATES COVERED** Master's Thesis	
4. TITLE AND SUBTITLE : Electromigration Related Effects At Metal-Metal Interfaces: Application To Railguns		**5. FUNDING NUMBERS**	
6. AUTHOR(S) William Bryant Cleveland Jr.			
7. PERFORMING ORGANIZATION NAME(S) AND ADDRESS(ES) Naval Postgraduate School Monterey, CA 93943-5000		**8. PERFORMING ORGANIZATION REPORT NUMBER**	
9. SPONSORING /MONITORING AGENCY NAME(S) AND ADDRESS(ES) N/A		**10. SPONSORING/MONITORING AGENCY REPORT NUMBER**	
11. SUPPLEMENTARY NOTES The views expressed in this thesis are those of the author and do not reflect the official policy or position of the Department of Defense or the U.S. Government.			
12a. DISTRIBUTION / AVAILABILITY STATEMENT Approved for public release; distribution is unlimited.		**12b. DISTRIBUTION CODE** A	

13. ABSTRACT (maximum 200 words)

This thesis had 2 objectives. The first purpose of this thesis was to develop an experimental procedure to study electric current induced flow of liquid metal, similar to that found at the armature-rail contact due to local melting, to determine the kinetics of liquid flow Ga under electric current conditions. For this, a model system comprising a bead of Ga on a Cu thin film track was devised in order to enable liquefaction and current induced movement of Ga to occur along the Cu track. Upon application of current, Ga underwent liquefaction due to Joule heating and once liquid, it rapidly migrated along the Cu track towards the negative terminal. The Ga liquid flow was attributed to electromigration of liquid Ga under the influence of direct electric field. The kinetics of Ga flow was determined. This method will be useful in calculating the kinetics of electromigration of molten Al along Cu rails in future railgun development. The second purpose of this thesis was to analyze debris left on Cu/24Ag rails following firing of 7075Al armatures, in order to understand the compositional evolution of the debris, and its role in creating surface damage to armature/rail interfacial surfaces. EDS analysis showed a majority of the debris was composed of oxidized aluminum with significant porosity. The analysis of the rail debris will benefit future studies on preventing rail debris from damaging railguns.

14. SUBJECT TERMS Railgun, Electromigration, Current Density, Thin Films			**15. NUMBER OF PAGES** 75
			16. PRICE CODE
17. SECURITY CLASSIFICATION OF REPORT Unclassified	**18. SECURITY CLASSIFICATION OF THIS PAGE** Unclassified	**19. SECURITY CLASSIFICATION OF ABSTRACT** Unclassified	**20. LIMITATION OF ABSTRACT** UL

NSN 7540-01-280-5500 Standard Form 298 (Rev. 2-89)
Prescribed by ANSI Std. 239-18

THIS PAGE INTENTIONALLY LEFT BLANK

Approved for public release; distribution is unlimited

ELECTROMIGRATION RELATED EFFECTS AT METAL-METAL INTERFACES: APPLICATION TO RAILGUNS

William Bryant Cleveland Jr.
Lieutenant, United States Navy
B.S., Thomas Edison University, 2000

Submitted in partial fulfillment of the
requirements for the degree of

MASTER OF SCIENCE IN MECHANICAL ENGINEERING

from the

NAVAL POSTGRADUATE SCHOOL
March 2007

Author: William Bryant Cleveland Jr.

Approved by: Indranath Dutta
Thesis Advisor

Anthony J. Healey
Chairman, Department of Mechanical and Astronautical Engineering

THIS PAGE INTENTIONALLY LEFT BLANK

ABSTRACT

This thesis had two objectives. The first purpose of this thesis was to develop an experimental procedure to study electric current induced flow of liquid metal, similar to that found at the armature-rail contact due to local melting, to determine the kinetics of liquid flow Ga under electric current conditions. For this, a model system comprising a bead of Ga on a Cu thin film track was devised in order to enable liquefaction and current induced movement of Ga to occur along the Cu track. Upon application of current, Ga underwent liquefaction due to Joule heating and once liquid, it rapidly migrated along the Cu track towards the negative terminal. The Ga liquid flow was attributed to electromigration of liquid Ga under the influence of direct electric field. The kinetics of Ga flow was determined. This method will be useful in calculating the kinetics of electromigration of molten Al along Cu rails in future railgun development. The second purpose of this thesis was to analyze debris left on Cu/24Ag rails following firing of 7075Al armatures, in order to understand the compositional evolution of the debris, and its role in creating surface damage to armature/rail interfacial surfaces. EDS analysis showed a majority of the debris was composed of oxidized aluminum with significant porosity. The analysis of the rail debris will benefit future studies on preventing rail debris from damaging railguns.

THIS PAGE INTENTIONALLY LEFT BLANK

TABLE OF CONTENTS

THIS PAGE INTENTIONALLY LEFT BLANK

LIST OF FIGURES

LIST OF TABLES

THIS PAGE INTENTIONALLY LEFT BLANK

ACKNOWLEDGMENTS

I would like to thank my advisor, Professor Indranath Dutta, for his guidance and encouragement throughout this project. I would like to thank Chadee Persad, Ramesh Guduru, Tiandan Chen, Chanman Park and Tom Christian for contributing their time and expertise. Finally, I would like to thank my family, Cathie, Kyle, and Megan, for their love, patience and support.

This research was supported by the Office of Naval Research MURI Grant # N00014-04-1-0599RQ-M and the National Science Foundation Grant # NSF-DMR 0513874.

THIS PAGE INTENTIONALLY LEFT BLANK

I. INTRODUCTION

A. ELECTROMAGNETIC RAILGUN

The U.S. Navy currently employs an arsenal of weaponry. Some which can bombard shoreline areas with total destruction and others which can go deep into enemy territory. Conventional guns, which are used on almost every navy ship deployed today, are relatively inexpensive to manufacture and good for short range targets. On the other hand, long-range weapons such as missiles and aircraft are extremely expensive to manufacture. Both weapon types are limited in the speed at which the weaponry can be launched.

The idea of using electricity to replace gun propellant might sound whimsical, but in fact, using electricity to launch projectiles can be dated all the way back to 1846 [1]. There is now substantial ongoing activity in designing a desirable electromagnetic (EM) railgun for use on board U.S. Navy ships. The principal advantage of a railgun is its very high muzzle velocity (approximately 2.5km/s) which results in a long strike range (approximately 300-400 nautical miles) [2,3].

The operation of a railgun is simple in principle. The railgun consists of two parallel metal rails, usually constructed of pure Cu or a Cu alloy, such as Cu/24Ag. The metal rails are made to be extremely conductive and are connected to an electrical power supply. A conductive projectile, usually made of an aluminum alloy, is inserted between the metal rails to complete an electric circuit. Electric current, in the range of 1 to 5 million amperes, is supplied from the positive terminal of the power supply to the positive rail. The current flows from the positive rail, across the armature, and back down the negative rail to the negative terminal on the power supply. The current flowing in the railgun creates an extremely large magnetic field in the region of the rails all the way up to the projectile. As current flows through the rails, based on the right hand rule, magnetic fields circulate around each rail. The current flows in opposite directions through the rails, which cause the net magnetic field to be vertical. With current flowing across the projectile horizontally, this causes a Lorentz force to be generated which will

accelerate the projectile along the rails and out the bore hole of the railgun. The Lorentz force is given by: $\vec{F} = \vec{j}X\vec{B}$ where $\vec{j}$ is the current density vector and $\vec{B}$ is the induced magnetic field vector. The schematic of a railgun along with the directions of $\vec{F}, \vec{B},$ and $\vec{j}$ are shown in Figure 1.

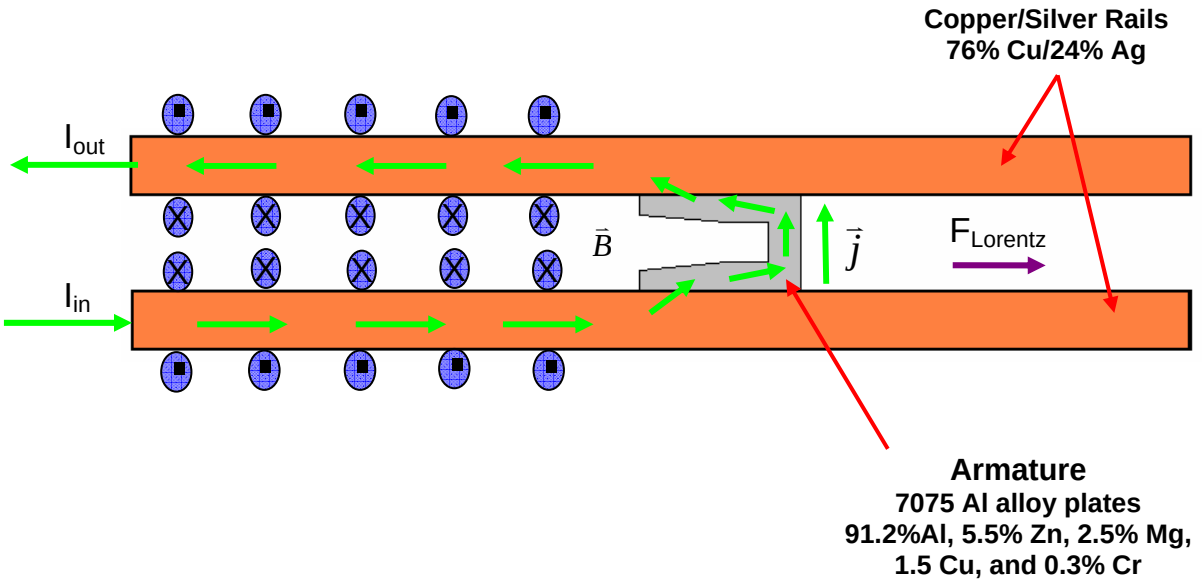

Figure 1. Schematic of basic railgun operation.

However, since the railgun comprises a hyper-velocity gliding metal-to-metal electromagnetic contact, it is subject to substantial interfacial damage. Melting and arcing damage of railguns occurs when the rails and armature loose contact during launch while the armature is traveling down the rails. A high temperature arc forms when contact is lost. The high-power-density arc causes damage to the rails in the form of surface melting [4, 5]. The surface melting left behind by arcing leads to layers of debris formed on the rails sliding surface. While the melting of metals acts as lubrication for sliding, the concern is when the layers of debris build up, leading to another form of railgun damage called plowing/gouging. Plowing occurs when the front portion of the armature gouges into the layers of debris left behind from previous shots. The damage caused by arcing is minimal compared to the damage caused by armature

plowing/gouging [6-14]. The possible flow of liquid aluminum on rails under electric current has also become a concern. This is known as electromigration. The study in this area is limited [15].

B. PURPOSE OF STUDY

This thesis investigates electro-mechanical effects at armature-rail contacts, related to tribology and electromigration, which can affect railgun life.

THIS PAGE INTENTIONALLY LEFT BLANK

II. BACKGROUND

A. ELECTROMIGRATION EFFECTS

1. Electromigration

Electromigration is the transporting of a material (i.e., metal) caused by slow movement of ions in a conductor due to the transfer of momentum from conducting electrons to diffusing metal atoms. The effect of electromigration is only important where high current densities are present. As the structure size of electronics decrease, this effect increases [34].

Material properties of metals have a strong influence on electromigration. The characteristics are primarily due to the composition of metal alloys and their dimensions. Other factors that affect electromigration are their shapes, crystallographic orientation of the grains, procedure for layer deposition, heat treatment or annealing, characteristics of the passivation ad the interface to other metals. There is also a difference with direct current or different alternating currents [34].

Electromigration occurs when the momentum of an electron is transferred to a nearby ion. The momentum transferred causes the ion to move from its original position. Over time, a large number of atoms will have been displaced from their original location. This can cause breaks, gaps or voids to form in the atoms original position [34].

The study of electromigration occurring in railguns has not been researched to date. Electromigration has been observed as far back as in the mid 1800's [16]. In the mid 1900's, electromigration systematic experimentations were conducted by Blech on thin films and studied using micro scale analysis [17-21]. Further study was conducted by Black [22] which found metal ions could be set free in their lattice by thermal activation. When the ions are set free, they become subjected to opposing forces. The "electric wind" force showed electrons pushing the metal ions in the direction of the anode while the "direct" force showed the current pushing metal ions towards the cathode. The stronger force was usually dependant on metal type, dimensions and current density. His research resulted in the ability to quantify electromigration and the

median time to failure by using $\frac{1}{MTF} = AJ^2 \exp\text{-}\frac{\phi}{kT}$. Where MTF is the median time to failure in hours, A is the cross sectional area of the device (cm^2), J is the current density (A/cm^2), φ is the activation energy (eV), k is the Boltzman's constant ($1.38x10^{-3}$J/K) and T is the temperature (°K).

Blech, during his research in thin films, derived an equation that modeled the atomic drift speed of atoms in the form of $v = \frac{J}{N} = \frac{D_0}{kT} eZ^* \rho j \exp\left(-\frac{\Delta H}{kT}\right)$. Where J is the atom flux ($moles/m^2s$), N is the density of metal ions ($moles/m^2$), D_0 is the frequency factor for diffusion (m^2/s), k is the Boltzmann's constant ($1.38x10^{-3}$J/K), T is the absolute temperature, eZ^* is the effective charge, ρ is the resistivity (Ω-cm(, j is the current density (A/cm^2), and ΔH is the activation energy (J) for moving defects in the metal. From the above equation, the atomic flux, J, can be calculated by using $J = \frac{ND}{kT} Z^* eE$ where the electronic charge and E is the electric field. The diffusion coefficient, D, is calculated using $D = D_0 \exp\left(-\frac{\Delta H}{kT}\right)$.

Results from Blech and Black's research allowed the derivation of many useful equations pertaining to electromigration. Blech's research further showed that current densities of 10^4 A/cm^2 were required to achieve electromigration in thin films. Current densities of 10^5-10^6 A/cm^2 showed a more severe and rapid electromigration effect. Blech determined that temperature, current density, specimen geometry and material have some effect on electromigration [18]. His research went on to show that thin film metals flow in the direction of electron flow due to "electric wind" forces dominating the field forces.

2. Surface Electromigration

Electromigration experiments have been conducted on very thin layers of metal (monolayers) which showed that electromigration can occur in the opposite direction of electron flow. This is known as surface electromigration. Yasunga and Notori conducted research showing a variety of results for surface electromigration occurring in very thin layers of metal on silicon substrates [22]. Their experiments consisted of silicon

substrates which were deposited with metal layers of 1-10 monolayers. The metal layers were heated to just below their melting point, to increase the mobility of the metal ions and to promote electromigration, by applying a current to the samples. The results showed electromigration occurring on the top layers of the metal samples where the ions are more loosely packed. Surface diffusion dominated grain boundary diffusion. Their testing showed that "direct" force became the dominating force when mobility of ions was increased which required current densities much less than in bulk or thin film electromigration experiments. They showed that electromigration could occur with current density as low as $10A/cm^2$.

In bulk or thin film electromigration, the "direct" force value is near unity and the electric wind component of the effective charge is a large negative value, thus, making the "wind force" the dominant driving mechanism. Bulk and thin film electromigration also requires large current densities in order for electromigration to occur. With surface electromigration, the surface layer has metal ions that are able to move and diffuse more freely than that in bulk or thin film metals, therefore, allowing electromigration to occur at a much lower current density. This allows the driving force of electromigration to be switched from "wind" force to "direct" force. As a low current density is applied to the monolayers, the mobility of metal ions is increased by Joule heating which allows the metal ions to flow in the direction of the cathode [23-25]. The total force acting on an ion is made up of the effective charge number, Z^*, the elementary charge, q, and the electric field, E. The can be calculated by using $F= Z^*qE$. The effective charge number Z^* breaks down into the electrostatic, Z_{el}, and wind, Z_w, in $Z^*= Z_{el}+ Z_w$.

Another difference between bulk/thin film electromigration and surface electromigration is the change in microstructure. When surface electromigration occurs, movement of the metal ions is more fluid-like in nature, transporting the top layers in its entirety as opposed to segmental movement. Therefore, very little microstructure damage occurs in surface electromigration. Conventional electromigration occurring in bulk/thin films, show electromigration flow in a more segmental movement. This causes pits and voids to form on the cathode side and hill-locks to form on the anode side, therefore, causing damage to the microstructure.

3. Electromigration in Liquids

Another facet of electromigration which is of interest is the study of electromigration of metals in liquid state. Research has been conducted on electromigration of several different liquid metals. One study, conducted by Anthony [26], addressed liquid metal inclusions in single crystal silicon. He created these metal inclusions by ultrasonically drilling holes with extremely small diameters in the substrate. Wires were inserted into the drilled holes, placed in an annealing furnace and heated for three hours to form liquid alloy inclusions. A current was applied to the sample causing the liquid metal inclusions to absorb silicon atoms. The inclusions were observed migrating towards the anode or cathode based on electric current. The absorbed silicon would transport the dissolved silicon atoms through the inclusions and deposit the silicon on the other side of the flux. This research showed that liquid metals will migrate towards the cathode by direct force.

Other research was conducted on electromigration and liquid alloys reinforcing the influence of an "electron drag" force. Epstein et al., [27] conducted research reinforcing this concept. When electrons passed through a liquid metal, the electrons hit the metal ions causing a "wind force". The liquid metal ions flow towards the direction of the cathode due to directional force being stronger than wind force. The electrons hitting the liquid metal ions moving the opposite direction causes a resistance in flow known as drag force.

A more relevant study was conducted by Regan et al., [28] on moving indium particles resting on carbon nanotubes by inducing an electric current. When the current was induced, it quickly raised the temperature of the indium to its melting point, due to Joule heating. Once the indium was molten, the liquid indium moved in the direction of current flow. The results were confirmed by reversing current flow in the opposite direction which caused the indium to reverse directions and flowed towards the new cathode. The transfer rate of the metal mass was controlled by varying voltage. This was attributed to direct force being the dominant field force.

Luc Delaney [15] conducted research on liquid metal electromigration. Observations were made on liquid aluminum flowing on a scaled down railgun model.

The rails were made of Cu, 1μm thick, coated on a silicon substrate. The two were separated by tantalum nitride to prevent the Si and Cu from reacting with each other. The armature used was made of Al-1100. The rail and armature were placed in a vacuum chamber which was modified to draw a high vacuum, therefore, prevent oxidation of Al. The sample was heated to just below the melting point of Al-1100 and a current of 4A was applied to the top rail , into the armature, and back out the bottom rail. The Al melted due to Joule heating and then flowed towards the cathode. The flow rate of Al was calculated to be 0.04mm/s. This was attributed to electromigration but required further research.

B. DEBRIS ON RAILS AFTER FIRING

There has been limited research regarding multi-shot wear debris. This research field has had tremendous growth over the last few years due to the impact of debris on railgun life. A study conducted by Persad et al., shows the debris is chemically complex and structurally inhomogeneous. Studies were done, following 1, 3 and 7 shot testing, without refurbishment of railgun rails. A square-bore, medium-caliber launcher (MCL) was used for all the tests. The test armature was a modified KJ design made from aluminum alloy with a polycarbonate bore rider. The rail contacts were made of a copper alloy. The specimens that were used for microstructural analysis were taken from the rail contacts one meter from the armature start position. The transit velocity at the specimen locations was approximately 2 km/s [13].

Analysis of rail after single shot was performed. The cross-section of the rail showed a thickness of the deposit layer of 40-60μm with porosity throughout the layer. The pore shapes were spherical with diameters ranging from 1-10μm. The three shot analysis displayed three distinguishable layers approximately 50μm thick. The top layer had noticeable more porosity and the armature/rail interface had the appearance of rail armature diffusive interaction. Seven shot results had a series of layers, dark and light, indicating a change in the rate of heat extracted from the melt. The thickness of the layer was 100μm and the armature/rail interface clearly displayed diffusive interaction. Porosity increased in the debris layer away from the armature/rail interface.

Porosity has been studied extensively [29-31]. It is believed the porosity comes from the dissociation of water at the surface of liquid aluminum. The hydrogen is left

behind to dissolve in molten aluminum while the oxygen reacts with aluminum. When the aluminum cools down, hydrogen gas pockets remain trapped in the solidified aluminum debris. Rail debris studies show the debris left on rails is Al_2O_3.

III. OBJECTIVE

This thesis has two objectives. The first objective is to develop an experimental procedure to study electric current induced flow of liquid metal, which is produced at the armature-rail contact due to local melting. For this, a model system comprising of Ga on Cu thin film was utilized in order to enable liquefaction and current-induced movement of the Ga melt to occur at low temperatures, and thereby allowing visual observation of the flow. Modifications were also made to a small scale, static model of a railgun, as used in reference [15], in order to allow measurements to be taken during the flow of liquid Ga along Cu rails for kinetic calculations. Based on these experiments, the kinetics of liquid flow under electric current were determined.

The second objective was to analyze the debris left on Cu/24Ag rails by 7075 armature following 1, 3, and 8 firings, in order to understand the compositional condition of the debris, and its role on causing surface damage of the rails. This was accomplished by sectioning the rails and inspecting the cross-sections of the debris-layers using optical microscopy, scanning electron microscope (SEM) and energy dispersive spectrometer (EDS).

THIS PAGE INTENTIONALLY LEFT BLANK

IV. EXPERIMENTAL PROCEDURE

A. EXPERIMENTAL SYSTEM FOR STUDYING FLOW OF LIQUIFIED GALLIUM ALONG CU TRACKS DUE TO ELECTRIC CURRENT

In order to study the kinetics of liquid flow under current, the experimental set-up comprised a Cu thin film rail or track, to which the electric current was applied, and a bead of Ga, which flowed along the Cu track following melting due to Joule heating.

1. Copper Track Construction

The rails were made from a silicon wafer, on which a Cu film of 1 μm thickness was electroplated, with a 70 μm thick TaN diffusion barrier layer between the Si and Cu. The silicon wafer was then cut into several pieces using a high speed cutting saw with a diamond blade. The cut pieces of the silicon wafer measured 6.72 mm wide by 31.27 mm long with a thickness of 0.71 mm. Parts of the Cu film were masked by placing 7 mm wide, 25 μm thick Kapton tape. The tape completely adheres to the pure Cu with overhang along the edges. Using an Exacto knife, the Kapton tape was cut to represent a rail with four leads branching off the rail. Once the cuts were complete, fine-tipped tweezers were used to remove the Kapton tape from the appropriate locations. The unmasked parts of the Cu film were then etched by placing in a beaker with 50 ml of an etching solution of 3 grams of $Na_2S_2O_8$ and 3% H_2SO_4 in 1000ml of DI H_20. The beaker was then agitated, ultrasonically, for approximately 15 minutes until the exposed Cu was etched away, leaving the desired rail. When the etching was complete, the sample was removed from the etching solution and rinsed in DI water and dried. The Kapton mask was carefully removed to expose the remaining Cu that was not etched away. The rail preparation was now complete, as shown schematically in Figure 2. The leads emerging from one side of the Cu-rail (Figure 2) are connected to a voltmeter, in order to monitor the flow of liquid metal as it progresses down the rail.

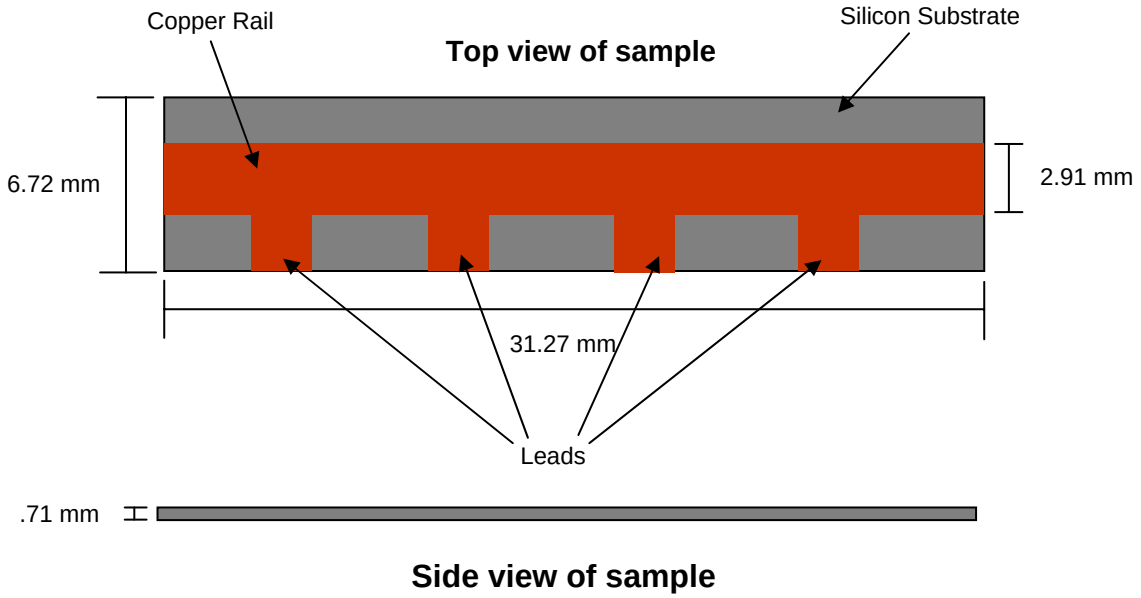

Figure 2. Top and Side view of prepared Cu track with leads after etching.

A bead of low melting metal (e.g. Ga) was placed at one end of the Cu-rail, before subjecting it to an electric current. In order for the experiment to work correctly, the low melting metal had to have a low enough resistivity to allow current to flow from the Cu rail, up into the Ga-bead and back out into the Cu rail. The resistivity of Ga is $14 \times 10^{-8}\Omega$-m, as compared with the resistivity of Cu, which is $1.7 \times 10^{-8}\Omega$-m [ ]. Therefore, for a Ga-bead to Cu-film thickness ratio of 1mm/1μm, i.e. 1000, the Ga to Cu resistance ratio is given by $(\rho_{Ga}t_{Cu})/(\rho_{Cu}t_{GA}) = 4.12 \times 10^{-3}$. Therefore, most of the current that passes through the Cu-rail, transitions into the Ga allowing us to study the effects of current induced flow of liquid Ga along the Cu track. Figure 3 shows a schematic of the rail with a bead of Ga at one end.

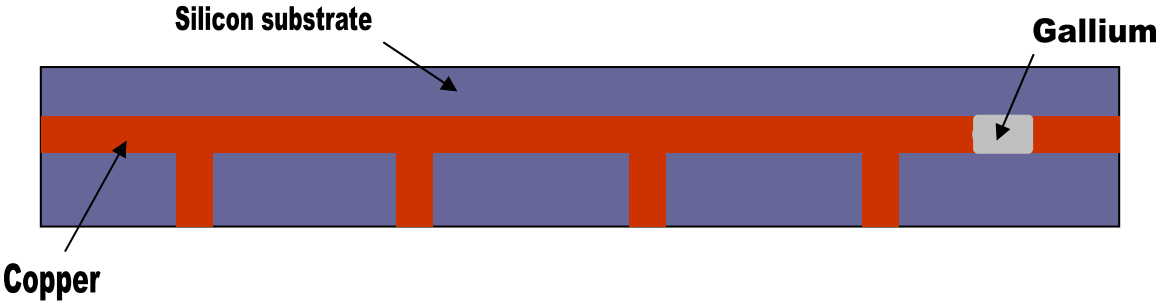

Figure 3. Cu track with Ga bead and leads branching off track.

2. System Design and Components

The track-bead system was placed inside a glass environmental chamber measuring 38cm x 20cm x 20cm, which was purged continuously with flowing Argon gas. Several feedthroughs into the glass box allowed electrical lead insertions, which not only allowed the introduction of current and voltage-measuring cables, but also connections for a heating device to heat the sample. A photograph of the environmental chamber is shown in Figure 4.

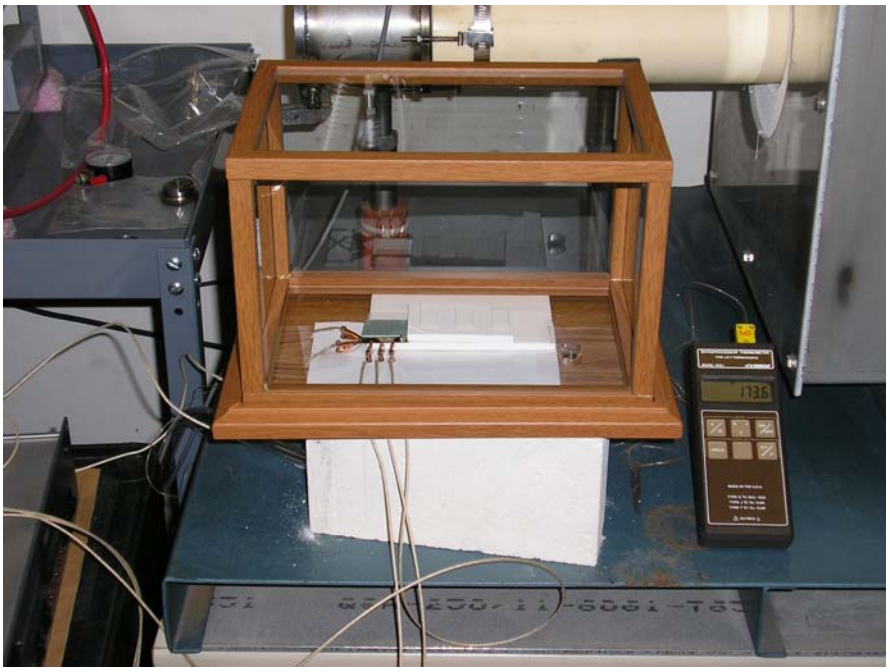

Figure 4. Picture of the environmental chamber with glass walls for viewing.

An Agilent E3632A power supply was used to apply a constant current range from 4A to 7A at the ends of the Cu rail. The power supply also provided a record of the voltage output at the ends of the two Cu rails.

An electric system was set up to measure the differential voltage across each adjacent lead on the rail of the Cu track as seen in Figure 5.

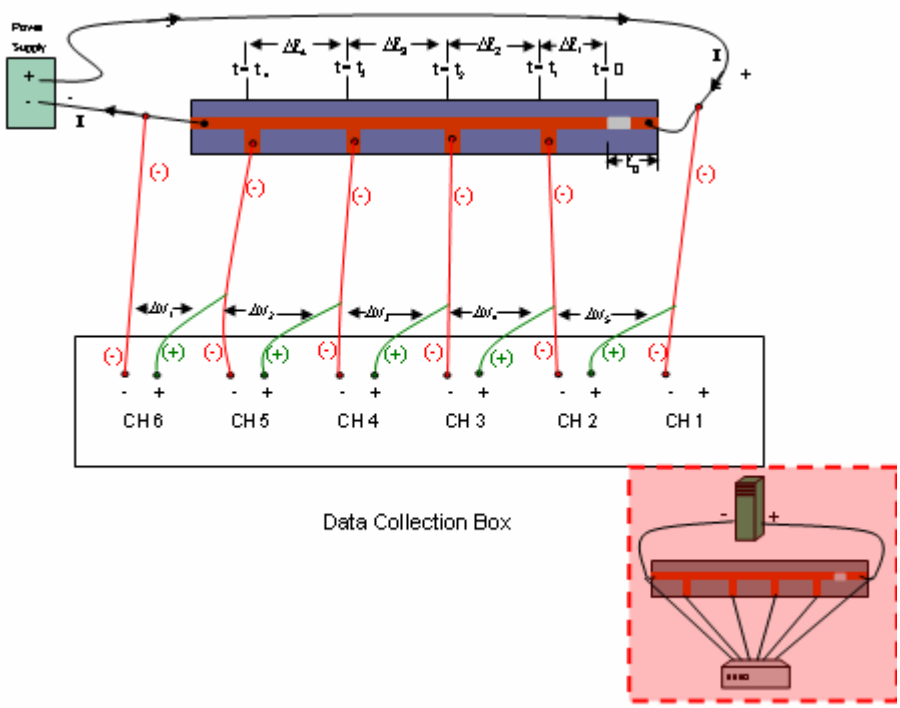

Figure 5. Schematic of differential voltage readings going to Data Collection Box.

For this, a National Instruments data acquisition card was utilized in conjunction with the software LABVIEW^{TM}. The differential voltage readings, were acquired every 500ms, with leads connected to the fingers emerging from one side of the Cu track. The electrical connection between the cables and the Cu-track were made using miniature, Cu spring clips. A thermocouple was placed in contact with the underside of the Si, just ahead of the location of the Ga bead to measure the temperature of the track. For one experiment, three thermocouples were placed at different locations along the track in order to assess the impact of temperature variations produced as the liquid Ga traveled along the track. A picture of the electrical system setup can be seen in Figure 6.

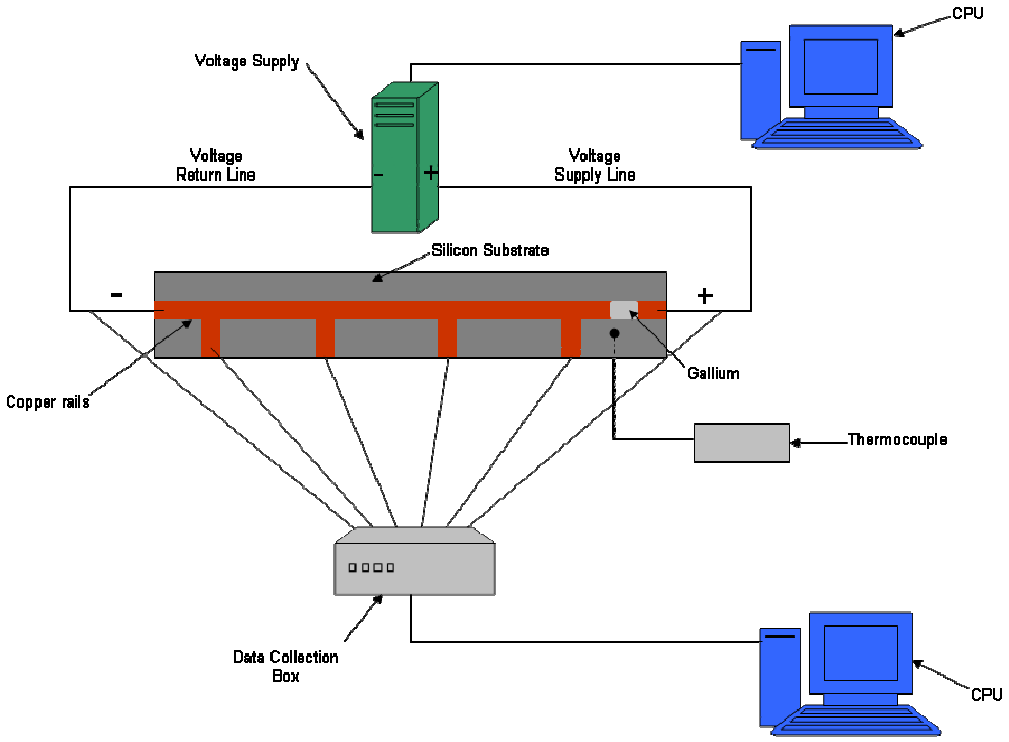

Figure 6. Basic System Setup with both electrical systems connected.

B. ANALYSIS OF RAIL SURFACE DEBRIS

Rail samples which had been fired 1, 3 and 8 times were provided by The University of Texas. The rail composition was 76% Cu and 24% Ag. The C-shaped armatures, used in firing, were made of 7075 Al. Rail samples were cut, longitudinally, in direction of armature movement using a water cooled, high speed cutting saw with a diamond blade. Cut pieces measuring 3mm x 5mm x 2mm were mounted in standard metallographic conductive epoxy as seen in Figure 7.

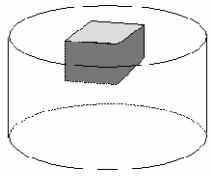

Figure 7. Cut rail sample mounted in metallographic conductive epoxy.

Samples were ground using 1000 grit SiC paper for 15 minutes in one direction. This was followed by another 15 minutes after sample was turned 90 degrees. These steps were repeated using 2000 grit SiC paper, 3000 grit SiC paper and 4000 grit SiC paper. The sample was then polished with 1 micron diamond paste for 40 minutes. The polishing process gave the cross-section of the sample a smooth mirror-like finish which was suitable for microscopic observation. Once sample preparation was complete, inspecting the cross-section of the debris-layers was carried out using Optical Microscopy, Scanning Electron Microscope and Energy Dispersive Spectrometer.

V. RESULTS AND DISCUSSION

A. MIGRATION OF LIQUID GALLIUM ON COPPER TRACK

As noted earlier, tests were performed for Ga migrating along Cu tracks using 5A, 6A and 7A at various ambient temperatures (22°C, 32°C, 47°C, 77°C, 122°C). Because of Joule heating, however, the actual temperature was substantially above the ambient. Besides, the track temperature also varied with time (i.e., flow of Ga). Based on the thickness of the Ga coating left on the track after the experiment, the cross-sectional area of the Ga layer was calculated for 5A, 6A and 7A. Assuming that nearly all current passes through Ga, current densities (j) of 1342 A/cm^2, 1475 A/cm^2 and 1750 A/cm^2 were obtained for applied currents of 5A, 6A and 7A respectively.

Tables 1-3 summarize the data for each experiment with applied current of 5A, 6A and 7A respectively. The current density, j, melt-front velocity, v, and the intermediate temperature, T, are listed at different times during each test, along with the natural log of velocities (ln v) and reciprocal temperature (1/T).

1. Summary of Test Data

Experiment	j(A/cm^2)		V(mm/s)		t(s)		T(°C)		Vavg	ΔT(°C)	lnV	1/T
Amb = 22°C I= 5 amps	1342	V_1	0.0181	t_1	380	T_1	128	± 106	0.0192	233-205	-4.0145	0.0025
	1342	V_2	0.0318	t_2	620	T_2	219	± 14		205-239	-3.4478	0.0020
	1342	V_3	0.0126	t_3	1010	T_3	199	± 7		205-239	-4.3762	0.0021

Table 1. Data from Experiments at 5A.

Experiment	j A/cm^2		V(mm/s)		t(s)		T(°C)		Vavg	ΔT(°C)	lnV	1/T
Amb=22°C I=6 amps	1475	V_1	0.0174	t_1	240	T_1	136	± 114	0.0170	22 - 250	-4.0524	0.0024
	1475	V_2	0.0225	t_2	472	T_2	227	± 23	± 0.0014	250 - 204	-3.7942	0.0020
	1475	V_3	0.0174	t_3	769	T_3	202	± 2		204 - 200	-4.0513	0.0021
	1475	V_4	0.0136	t_4	1144	T_4	181	± 19		200 - 162	-4.2999	0.0022
Amb=32°C I=6 amps	1475	V_1	0.0117	t_1	394	T_1	122.5	± 90.5	0.0085	32 - 213	-4.4460	0.0025
	1475	V_2	0.0138	t_2	763	T_2	197.5	± 15.5	±0.0017	213 - 182	-4.2838	0.0021
	1475	V_3	0.0067	t_3	1597	T_3	162.5	± 19.5		182 - 143	-5.0059	0.0023
Amb=47°C I=6 amps	1475	V_1	0.0139	t_1	373	T_1	112.5	± 65.5	0.0136	47 - 178	-4.2751	0.0026
	1475	V_2	0.0173	t_2	663	T_2	169	± 9	±0.0018	178 - 160	-4.0588	0.0023
	1475	V_3	0.0108	t_3	1016	T_3	152	± 8		160 - 144	-4.5264	0.0024
Amb=77°C I=6 amps	1475	V_1	0.0229	t_1	180	T_1	194.5	± 117.5	0.0271	77 - 312	-3.7747	0.0021
	1475	V_2	0.0347	t_2	345	T_2	298.5	± 13.5	± 0.0015	312 - 285	-3.3620	0.0017
	1475	V_3	0.0246	t_3	565	T_3	277	± 8		285 - 269	-3.7035	0.0018
	1475	V_4	0.0251	t_4	775	T_4	263.5	± 5.75		269 - 258	-3.6851	0.0019
Amb=122°C I=6 amps	1475	V_1	0.0275	t_1	197	T_1	169.5	± 47.5	0.0097	122 - 217	-3.5932	0.0023
	1475	V_2	0.0173	t_2	445	T_2	213	± 4	±0 .0017	217 - 209	-4.0547	0.0021
	1475	V_3	0.0137	t_3	771	T_3	205	± 4		209 - 201	-4.2873	0.0021
	1475	V_4	0.0062	t_4	1542	T_4	197.5	± 3.5		201 - 194	-5.0789	0.0021

Table 2. Data from Experiments at 6A.

Only one test was conducted at 5A. At 6A, problems were encountered at two temperatures. At 32°C and 47°C, the migration of Ga along the Cu rail, became very slow after some time, possibly because of entrance melt viscosity due to oxidation and/or alloying with Cu.

Experiment	j A/cm^2		V(mm/s)		t(s)		T(°C)		Vavg	ΔT(°C)	lnV	1/T
Amb = 22°C I= 7 amps	1750	V_1	0.0195	t_1	207.5	T_1	87	± 65	0.02158	22-151	-3.9389	0.0028
	1750	V_2	0.0346	t_2	374	T_2	145	± 7	± 0.00413	151-138	-3.3641	0.0024
	1750	V_3	0.0324	t_3	561.5	T_3	126	± 12		138-114	-3.4304	0.0025
	1750	V_4	0.0123	t_4	967	T_4	104	± 10		114-94	-4.3977	0.0027
Amb = 26°C I= 7 amps	1750	V_1	0.0112	t_1	163.5	T_1	142	± 116	0.00841	26-257	-4.4925	0.0024
	1750	V_2	0.0156	t_2	456.5	T_2	271	± 14	±0.00141	257-284	-4.1607	0.0018
	1750	V_3	0.0106	t_3	1021	T_3	259	±26		284-233	-4.5466	0.0019
	1750	V_4	0.0052	T_4	1915	T_4	205	± 29		233-176	-5.2637	0.0021
Amb = 38°C I= 7 amps	1750	V_1	0.0051	t_1	515	T_1	105	± 67	0.00604	38-173	-5.2848	0.0026
	1750	V_2	0.0060	t_2	963.5	T_2	167	± 5		173-162	-5.1090	0.0023
Amb = 53°C I= 7 amps	1750	V_1	0.0150	t_1	220.5	T_1	155	± 102	0.01672	53-257	-4.1989	0.0023
	1750	V_2	0.0167	t_2	318	T_2	275	± 18		257-294	-4.0913	0.0018
Amb=74°C I=7 amps	1750	V_1	0.0232	t_1	109	T_1	205	± 131		74-336	-3.7631	0.0021
Amb=128°C I=7 amps	1750	V_1	0.0269	t_1	91.5	T_1	274	± 146	0.03481	128 - 420	-3.6162	0.0018
	1750	V_2	0.0348	t_2	170.5	T_2	485	± 65		420-550	-3.3578	0.0013

Table 3. Data from Experiments at 7A.

At 7A, several problems were encountered. During testing at 26°C and 128°C, the Cu rails lost continuity due to excessive heating and burn-out after some period of time. Samples also underwent burn-up at 38°C, 53°C and 74°C, after some time, preventing Ga from flowing the full length of the rails. Therefore, only the data collected prior to the failure was used for the flow kinetics. The reason for this burn-out is not clear, although it can be surmised that oxidation of the Ga and alloying with Cu, enhance the resistance of the liquid front and caused excessive heating, and ultimately, failure of the Cu track.

2. Testing Results of 6A at 122°C

All the data listed in the previous three tables were collected and analyzed in the same manner. An in-depth look at the 6 Ampere test with ambient temperature of 122°C is provided below.

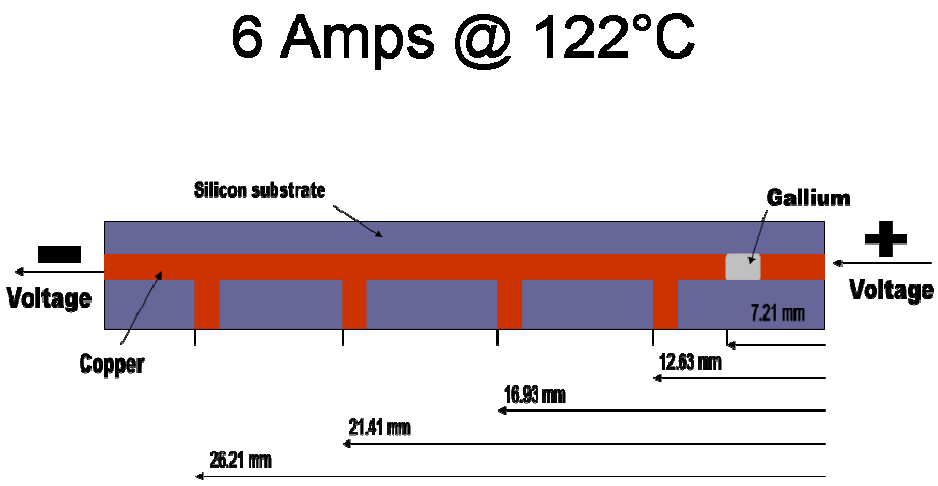

Figure 8. Schematic of sample used for 6A with Cu lead measurements, Ga position, and voltage direction @ 122°C ambient temperature.

Figure 8 shows a schematic of the sample used for the experiment at 6A and 122°C, along with the direction of current flow. The Cu thin film track is 2 mm wide, with a thickness of 1μm. There are 4 Cu leads branching off the main Cu rail, which were connected to a multi-channel volt meter card. As the Ga melted and flowed across the Cu rail, it triggered a change in the differential voltage measured at each of these branches, thereby producing a record of the location of the Ga flow front at different times. Photographs showing the progress of the Ga melt-front during an experiment are shown in Figure 9. The top left picture shows the setup without Ga. The top right picture shows the setup with Ga. As current is supplied to the sample, Ga starts to flow across the Cu rail. The remaining six pictures show, from left to right, continuing down the page, how Ga flowed and triggered the leads.

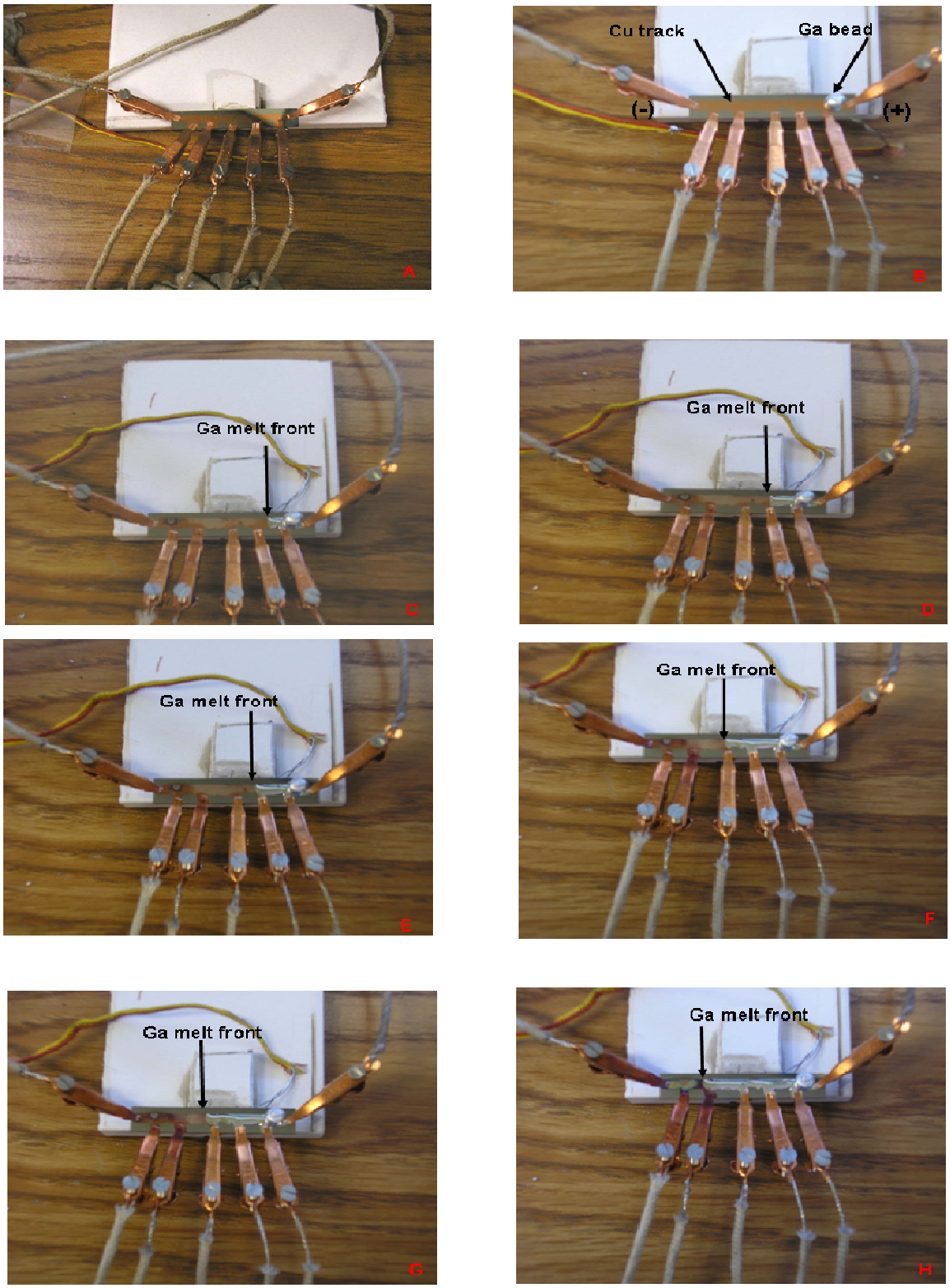

Figure 9. Photographs showing progression of electromigration from A-H during 6A experiment with arrow showing Ga melt front.

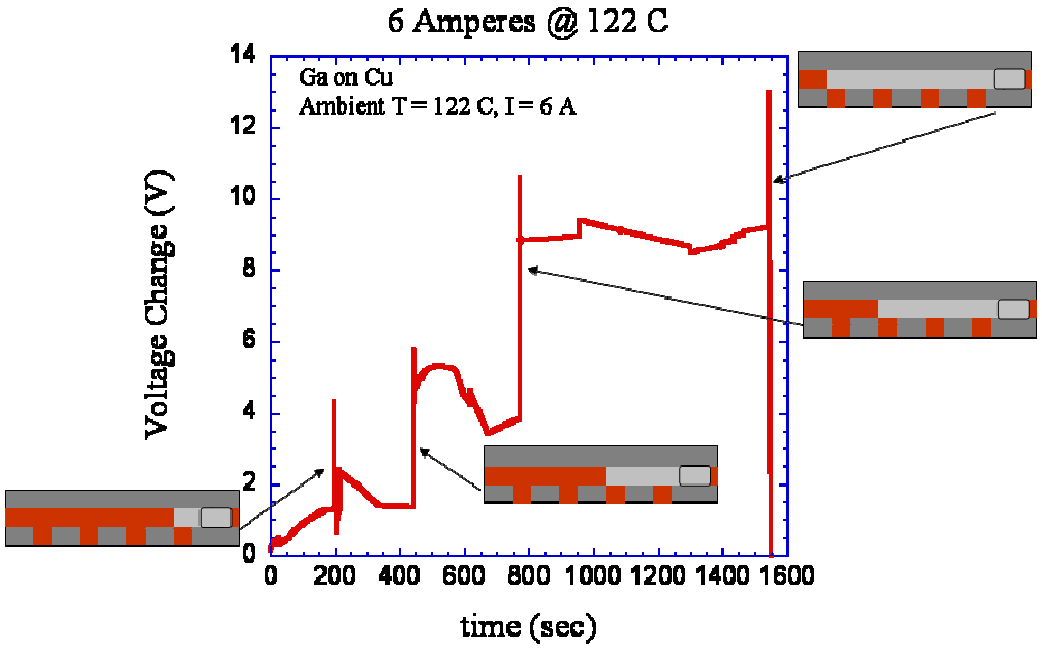

Figure 10. Differential voltage readings showing jumps where Cu leads were covered by Ga melt front with respect to time.

Figure 10 shows the change in voltage that occurred between leads while conducting the experiment. A constant current of 6A was supplied to the Cu rail. Once current was supplied to the sample rail, the Ga began to heat up due to Joule heating, underwent melting, and started flowing in the direction of current flow (i.e., anode to cathode). As the Ga flowed past the first lead branching off the Cu rail, the Ga sealed off the first loop and caused a jump in voltage change. This can be observed in Figure 10. As the Ga continued to flow towards the (-) Cathode, it continued to pass leads and cause jumps in voltage change. After the Ga reached the end of the rail, the experiment was stopped. The voltage change data was combined with the previous measurements taking on the rail to determine the distance the Ga traveled with respect to time.

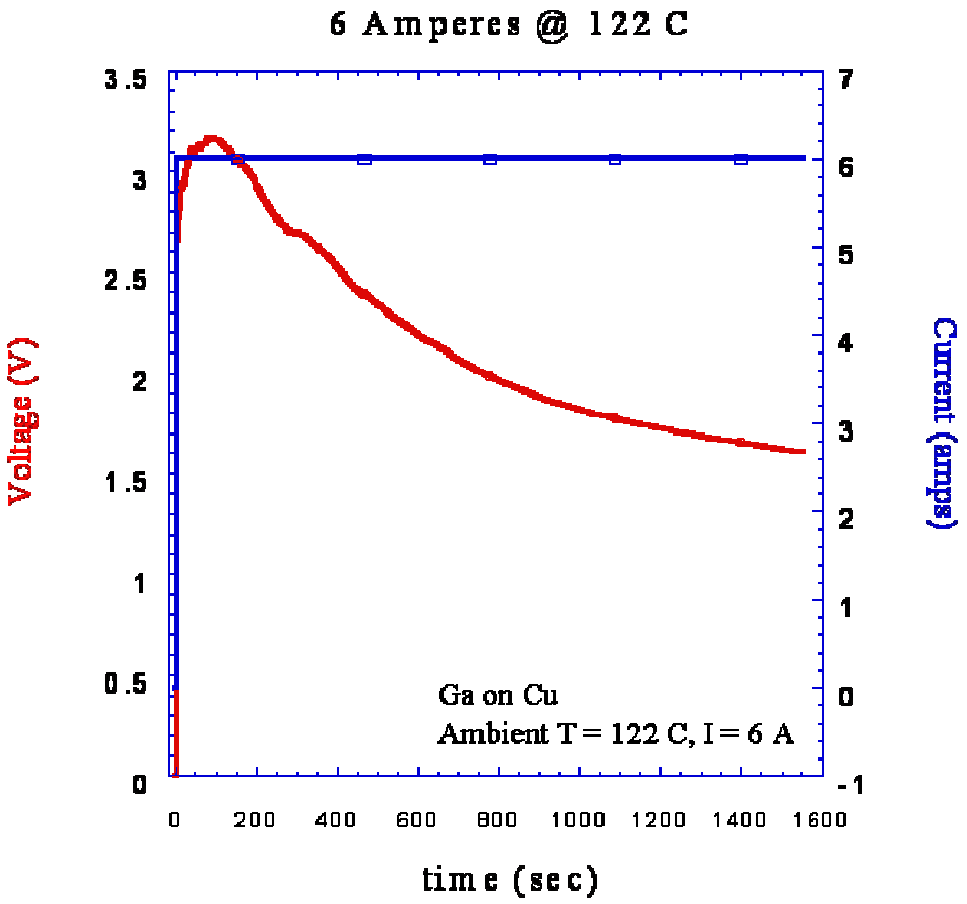

Figure 11. Voltage and Current graphed with respect to time during 6A analysis at ambient temperature of 122°C.

Voltage and current were plotted as seen in Figure 11. The figure shows that while a constant current was maintained, voltage initially rose, and then steadily decreased throughout the duration of the experiment. The initial rise is attributed to an increase in resistance due to the increase in temperature as the Cu track undergoes Joule heating. As the Ga bead melts and spreads along the Cu track towards the cathode, the effective cross-section of the conductor increases due to the coating of Cu by Ga, resulting in a decrease in resistance, and hence the voltage. This is clear by comparing Figure 11 with Figure 12 which plots the temperature variation with time. The trends are very similar, indicating that the voltage change is associated with the flow of Ga.

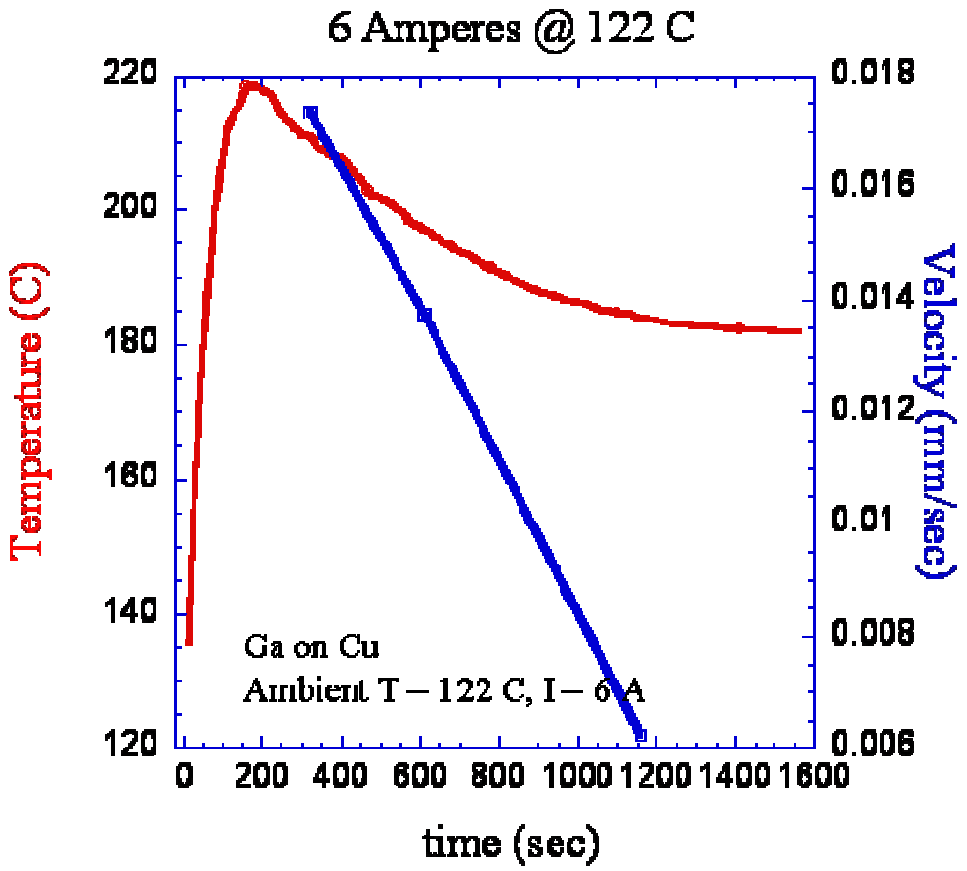

Figure 12. Temperature and Velocity graphed with respect to time during 6A experiment at ambient temperature of 122°C..

When the Ga starts to flow, creating a parallel circuit, the resistance drops causing voltage to drop, which in turn leads to a drop in temperature. The change in temperature lags slightly behind voltage changes due to temperature not being able to react to the changes as quickly as voltage. Velocity was plotted based on the distance the Ga traveled with respect to time. Velocity drops with time due to the associated drop in temperature. Thus, the flow rate appears to be dependant on temperature. An additional reason for the drop in velocity with time could be the increased viscosity of the liquid Ga associated with alloying and/or oxidation.

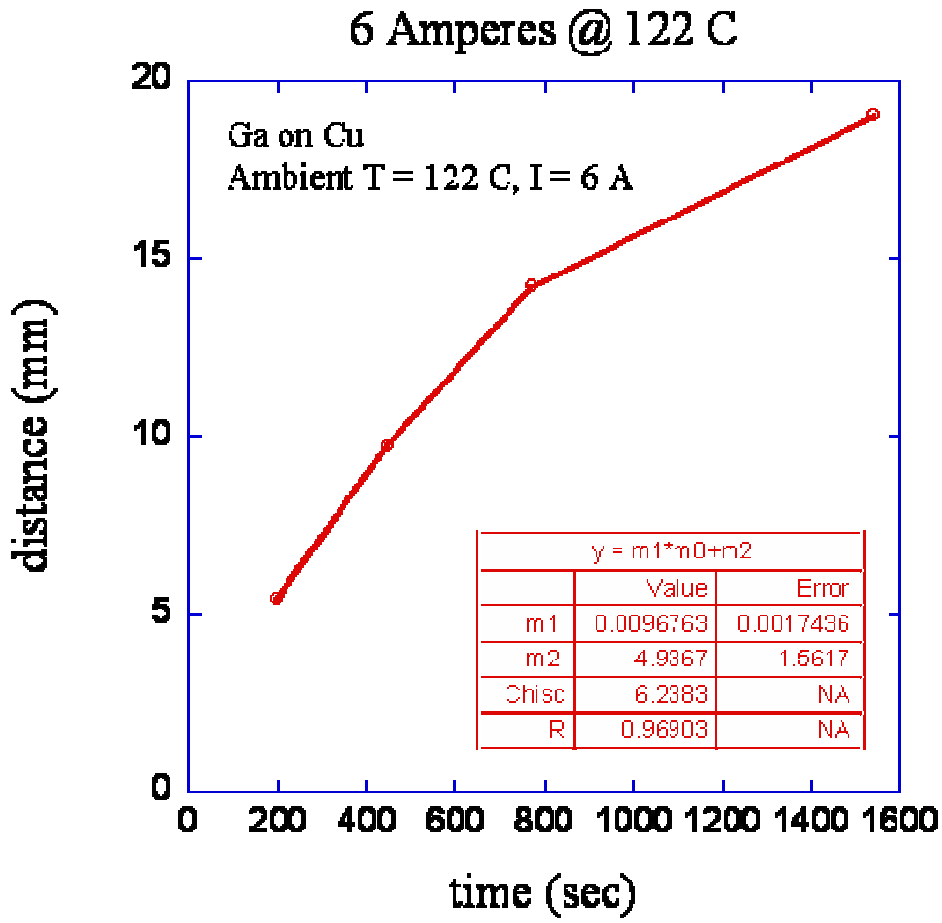

Figure 13. Distance graphed with respect to time during 6A experiment including slope table at ambient temperature of 122°C..

The velocities were calculated from the data collected from the differential voltage versus time measurements (Figure 10), from which, the distance versus time graph, (Figure 13), were produced. The slope of the distance versus time graph gave the average velocity of Ga during flow. Since the velocities are sensitive to temperature, the mean temperature for each velocity reading is listed in Tables 1-3.

In order to ascertain whether the observed flow rate of Ga is governed by a diffusional process showing an Arrhenius dependence on temperature, the lnV data from all the experiments at 6A were plotted against the reciprocal of the mean temperature (1/T), as shown in Figure 14.

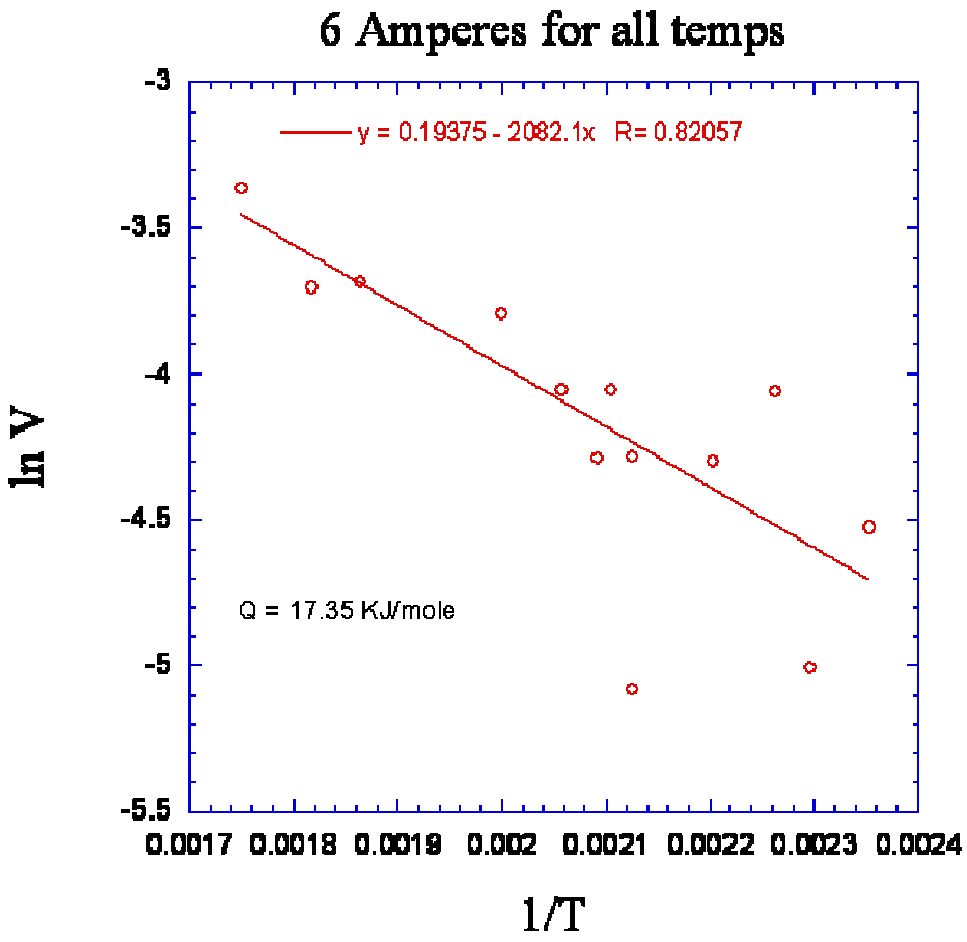

Figure 14. lnV with respect to 1/T for all temperatures at 6A.

Although there is significant scatter in the temperature data because of the uncertainty of the actual temperature at the melt-front, the lnV versus 1/T data shows a reasonable fit to a straight line, indicating that velocity has an Arrhenius dependence on temperature. The activation energy of Ga from these experiments was determined to be 17.35 kJ/mole.

The self diffusivity of liquid Ga between 292°C - 556°C is given by $D=2.2\times10^{-10}T^2$ [32]. Plotting this data as lnD versus 1/T one obtains an activation energy of 19.06 kJ/mole as seen in Figure 15.

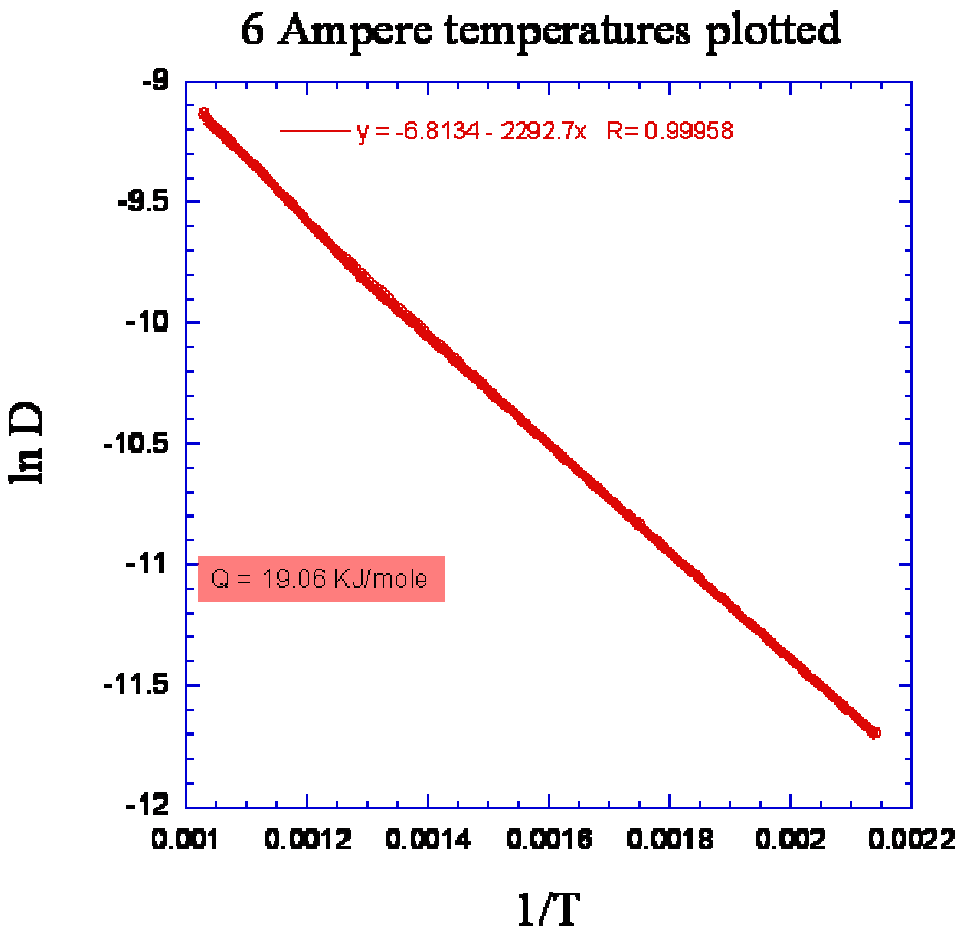

Figure 15. ln D versus 1/T using existing equation for activation energy of Ga.

Thus, the activation energy measured in the present study is quite close (within ~9%) of the activation for Ga self diffusion in the liquid state. Since the observed flow is associated with current flow, it is therefore likely due to electromigration.

To further ascertain whether the flow of liquid Ga along the Cu track is due to electromigration, additional testing was required. The flow of Ga could be caused by electromigration, thermomigration or a combination of the two. Past experiments show that electromigration occurred in bulk and thin film metals when an electric current of 10^4 A/cm^2 or greater was induced. The metal flowed in the direction of the anode due to "wind" force dominating "direct" force. This is caused by the electric wind current having a large negative value and direct force value being near unity [17-21]. Further studies of electromigration were conducted on monolayers and liquid metals showing that

electromigration caused flow, in the opposite direction, towards the cathode with current densities as small as 10 A/cm^2. The metal flow, towards the cathode, was due to the presence of mobility. In bulk and thin films, the metal is restricted by the crystal structure. This dramatically reduces the mobility of the bulk and thin film metals preventing the "direct" force from being dominant. In monolayers and liquid metals, the crystal structure does not restrict mobility. In monolayers, the surface ions have significant mobility and the liquid metals have free mobility in all directions. This allows the "direct" force to dominate [15, 22-28]. These studies further support liquid Ga flow was caused by "direct" force electromigration.

Temperature was measured in 3 different locations below the silicon substrate as seen in the figure below. All three temperature measurements were measured by a thermocouple temperature measuring device.

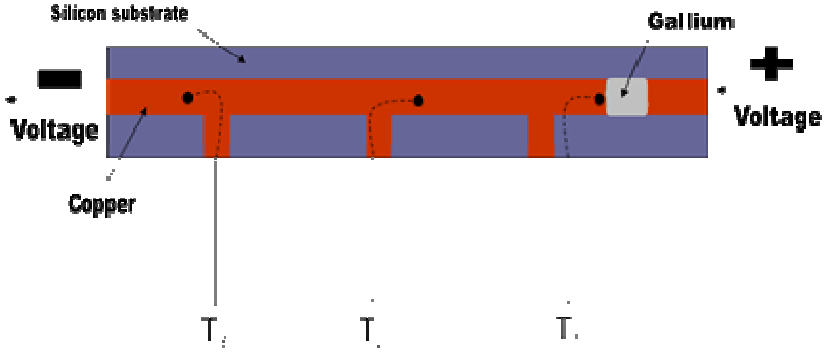

Figure 16. Schematic of sample with temperature measurements in 3 locations.

To verify Ga flow was due to electromigration and not thermomigration, a test was set up to measure the temperature of the Cu track, in several locations, while a bead of liquid Ga flowed down the rail. Figure 16 is a schematic of the setup. Three temperature measurements were taken at different locations along the track and plotted on a graph shown in Figure 17.

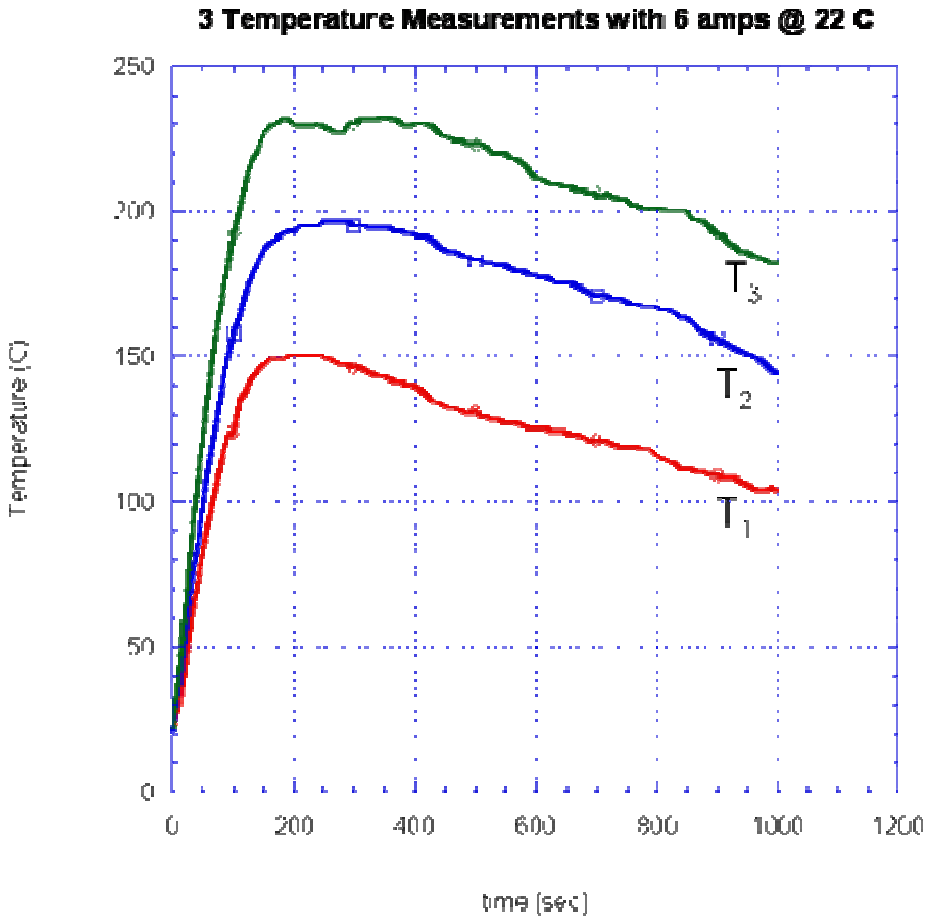

Figure 17. Graph showing temperature changes over time at 3 points along sample.

The test showed a large temperature gradient was created along the Cu track. The lower temperature measurements were at the end of the Ga and the higher temperature readings were taken at the end furthest away from Ga bead. This temperature gradient was caused by Joule heating along the Cu rail due to resistivity of Cu. Areas along the Cu track where Ga was present showed temperature reading much lower due to the drop in resistivity. This test raised suspicion that flow might be from thermomigration.

A second test was set up placing the Ga bead in the middle of the Cu track. If the liquid Ga flow was due to a temperature gradient, then the bead should not move in either direction. Both ends of the copper track would have a higher temperature than the middle of the track where the Ga bead was placed. Once current was introduced to the sample, the Ga bead underwent melting and began to flow towards the Cathode. This test verified

that the flow of liquid Ga that occurred in the previous tests were in fact due to "direct" force electromigration. The test results can be seen at three different times in the schematic below (Figure 18).

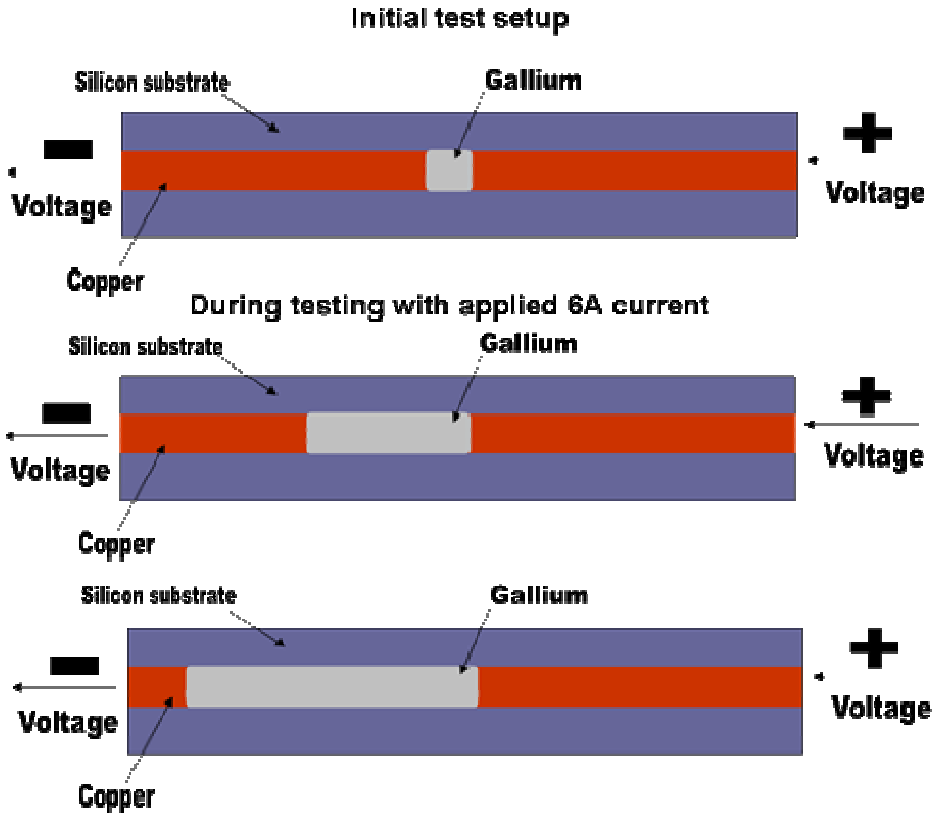

Figure 18. Schematic of samples at various stages in temperature gradient testing.

B. ANALYSIS OF SLIDING SURFACE OF LAUNCHED RAILS

Three railguns were fired 1, 3, and 8 times using C-shaped 7075 Al armatures respectively at IAT, UT Austin. The rails were removed and cut into sample pieces along the rail/armature interface, and the longitudinal cross-section of the rail were to analyze the debris on the rails, as shown in Figure 19.

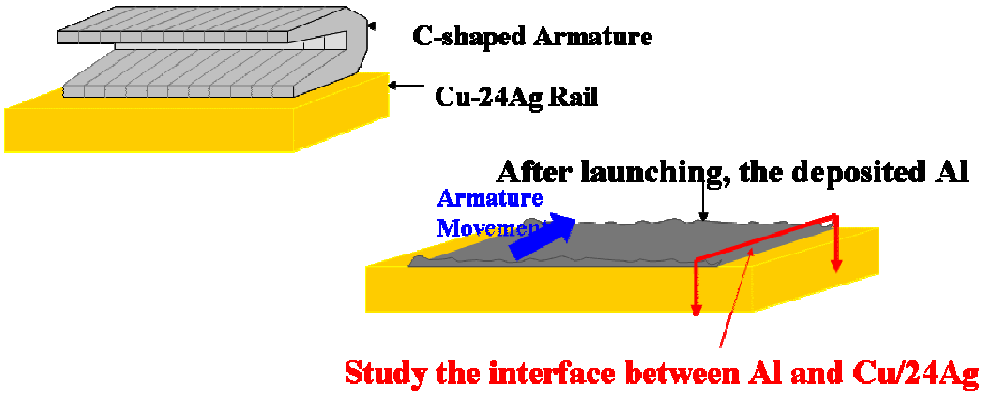

Figure 19. Armature construction diagram and interface direction studied.

The debris was studied at several different moments in time. The cross-sections were then mounted and ground/polished for observation. Optical Microscopy was initially used to ensure samples were prepared correctly and debris was located. After completing the Optical Microscopy analysis, the samples were then placed inside the SEM. Studying of samples took place in the SEM. EDS was then used to identify the constituents of the debris. The constituents were then plotted to show element composition change throughout the layers. The results from various shots studied are listed below.

1. Rail Cross-Section after 1 Shot

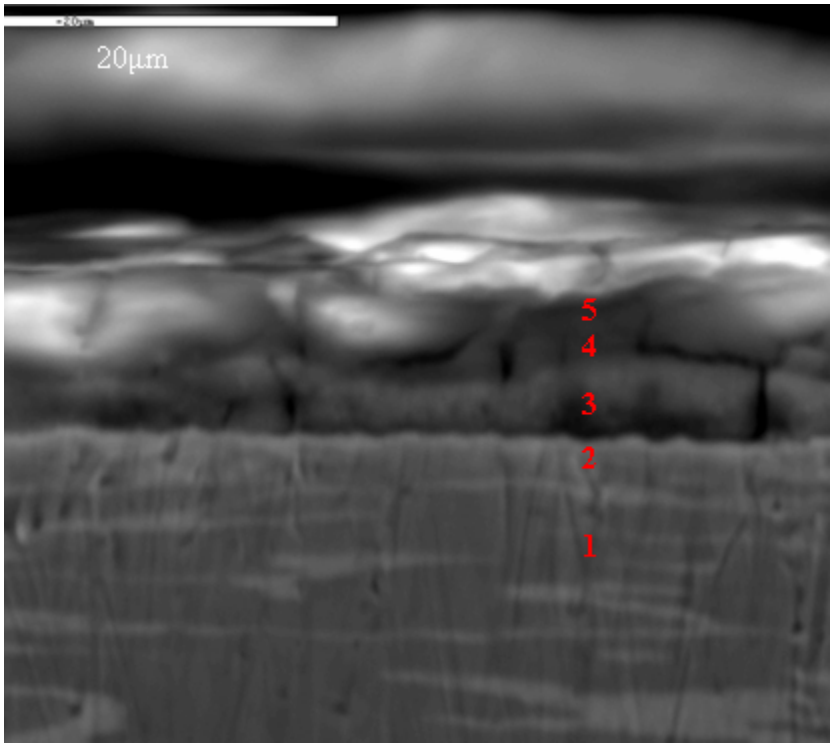

Figure 20. SEM picture of cross-section of rail for 1 shot.

After 1 shot, the average thickness of the debris ranges from 10-23µm. There was very little damage to the Cu-24Ag rail surface. The aluminum layers were solid in form with regions showing porosity. Most of the pores were approximately 2-4.5µm in diameter and scattered in various regions along the debris. The interface between the deposited layer and the Cu-24Ag rail was smooth and sharp with little or no rail damage. This indicated no mechanical or chemical damage occurred over most of the rail surface. Figure 20 shows a picture taken using the SEM that was then analyzed by EDS. Figures 21-25 show the EDS graphs with compositional charts at various points shown in Figure 20.

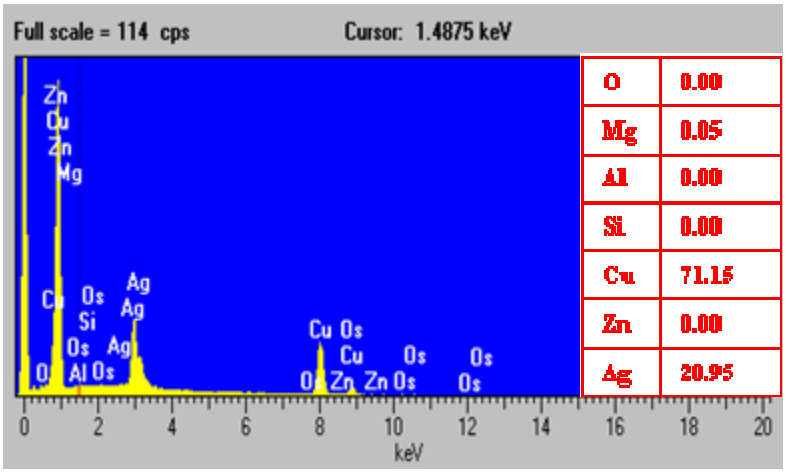

Figure 21. EDS analysis of point 1 for 1 shot.

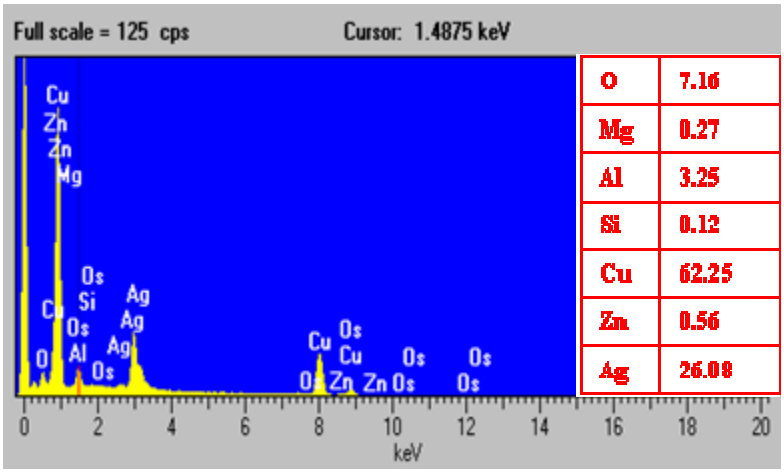

Figure 22. EDS analysis of point 2 for 1 shot.

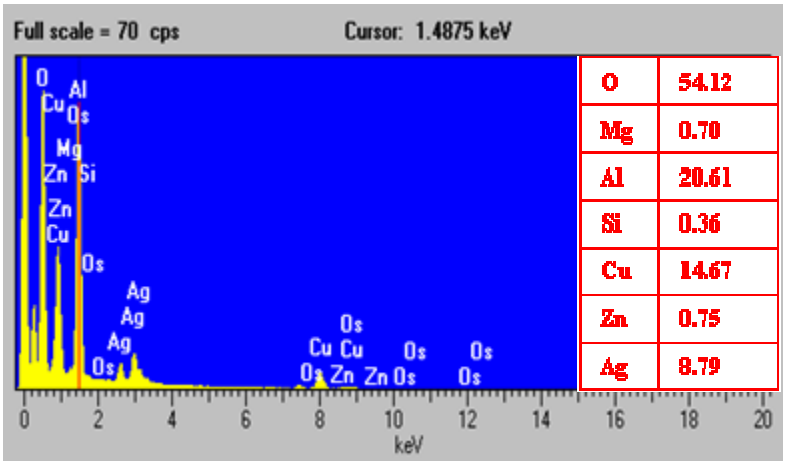

Figure 23. EDS analysis of point 3 for 1 shot.

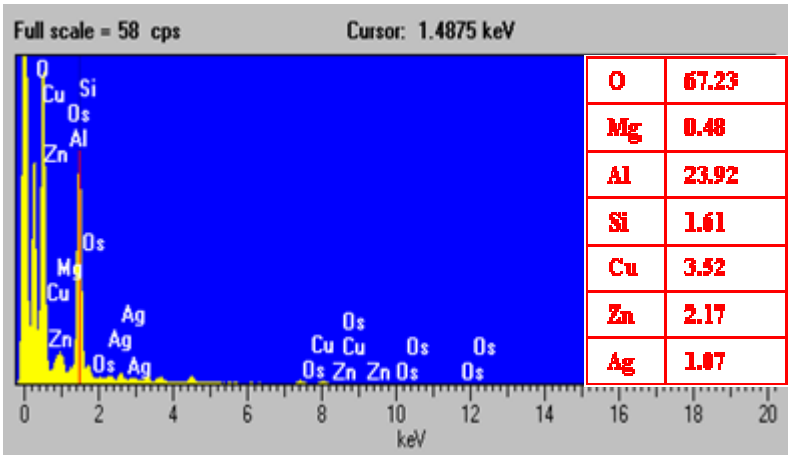

Figure 24. EDS analysis of point 4 for 1 shot.

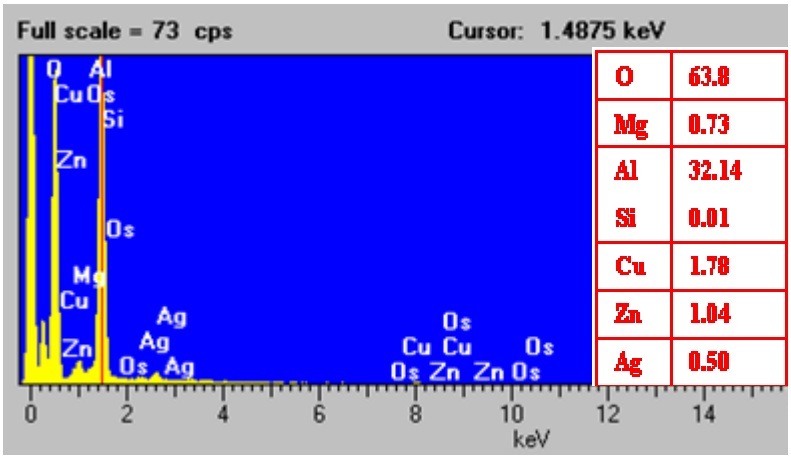

Figure 25. EDS analysis of point 5 for 1 shot.

The combined results from the EDS analysis on the 1 shot rail sample are displayed in Figure 26. The results were plotted on one graph for ease of analysis. At point 1, the EDS analysis was taken 15μm below the rail surface. Expected element concentration levels were found at point 1. At point 2, on the edge of the rail, Cu and Ag concentrations decrease as Al and O concentrations increase. This is caused by melted aluminum reacting with the atmosphere (oxygen) to form Al_2O_3 [13]. Very little diffusion takes place between the debris and the rail, hence, the constant decline in Cu and Ag between points 2 and 3. At point 3, 4, and 5, a small amount of Cu and Ag exist in the debris. This is caused by diffusive interaction, although not apparent when analyzing armature/rail interface in SEM. Al and O concentrations continually increase due to the abundance of atmospheric gases and moisture present inside the railgun.

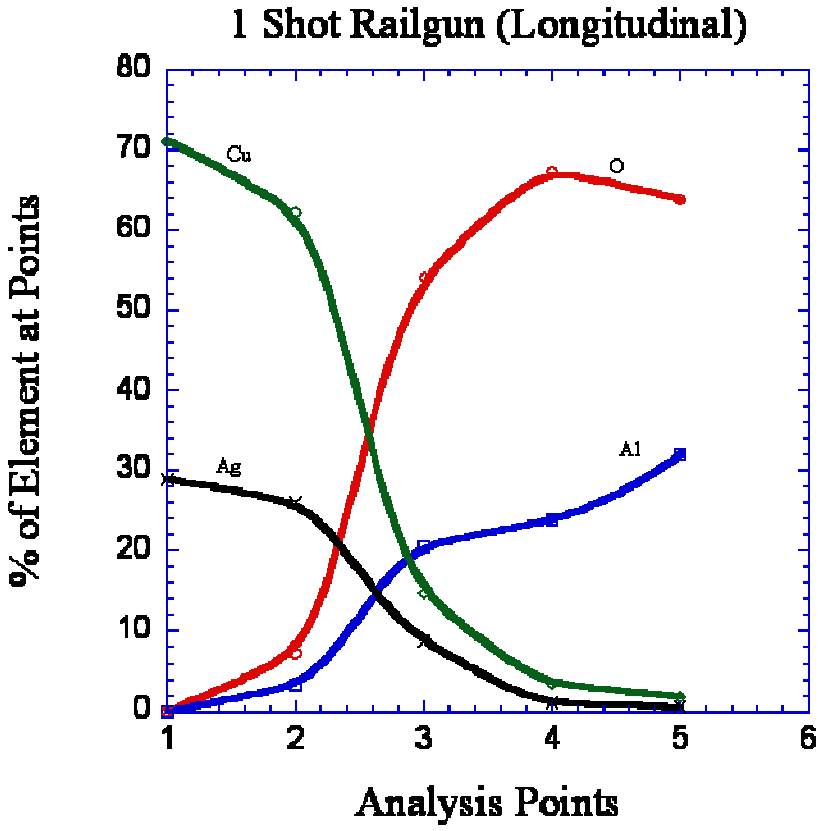

Figure 26. Combined element concentration graph for 1 shot.

2. Rail Cross-Section after 3 Shots

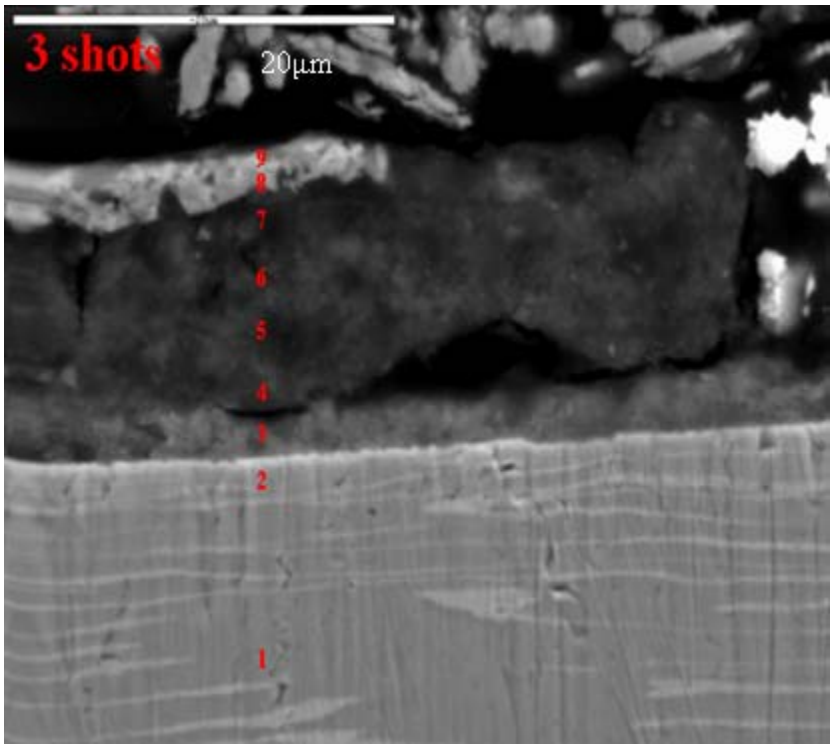

Figure 27. SEM picture of cross-section of rail for 3 shots.

After 3 shots, only minor changes were observed relative to 1 shot. There were clearly three sandwich-like layers of debris on the rail. The thickness of the debris measured 22μm with the top layer measuring 5μm and the bottom two layers measuring 17μm. Porosity was throughout the debris, increasing in diameter size towards the top of the debris layer. The top layer had more vertical cracks than the bottom two layers and appeared to be brittle. The interface between debris layer and rail became distorted, indicating possible diffusive interaction occurring between rail and armature. The increase in shots caused the rail surface to become uneven with mechanical damage or chemical reaction. The rail appeared to be undamaged where all three layers of debris were present. Figure 27 shows a picture taken using the SEM that was then analyzed by EDS. Figures 28-36 show the EDS graphs with compositional charts shown at various points as shown in Figure 27.

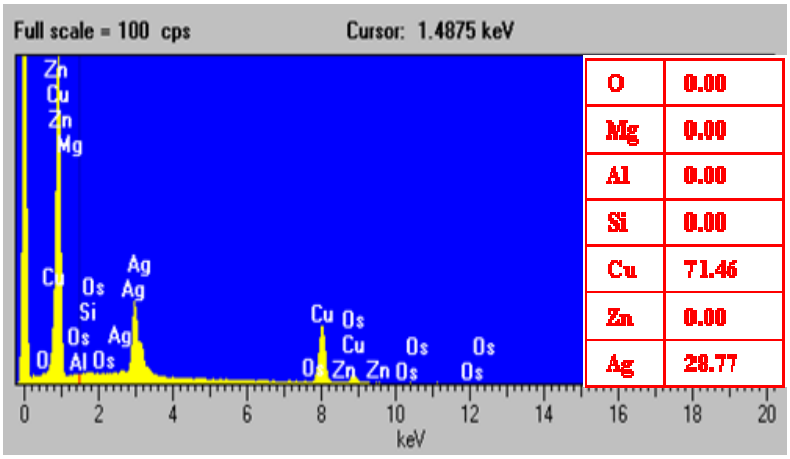

Figure 28. EDS analysis of point 1 for 3 shots.

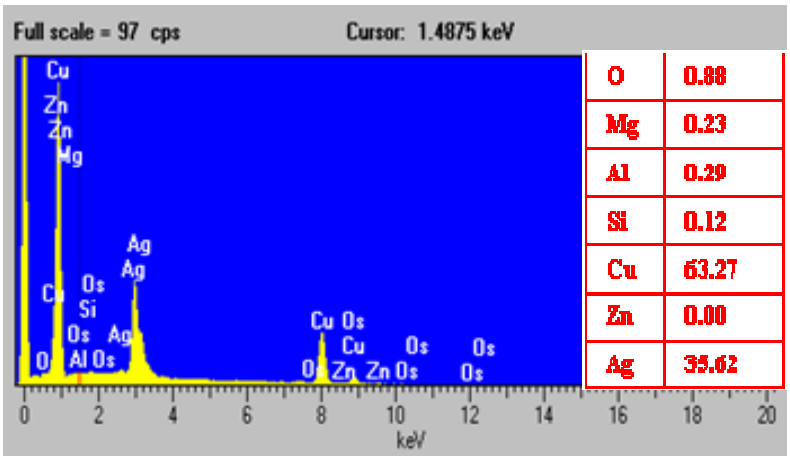

Figure 29. EDS analysis of point 2 for 3 shots.

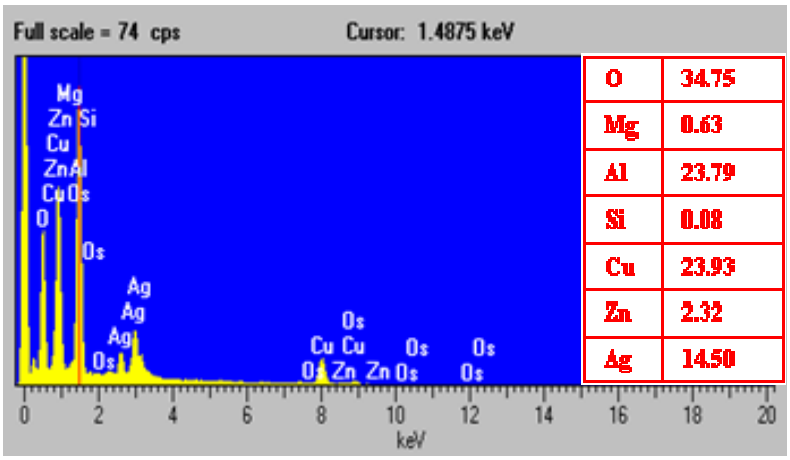

Figure 30. EDS analysis of point 3 for 3 shot.

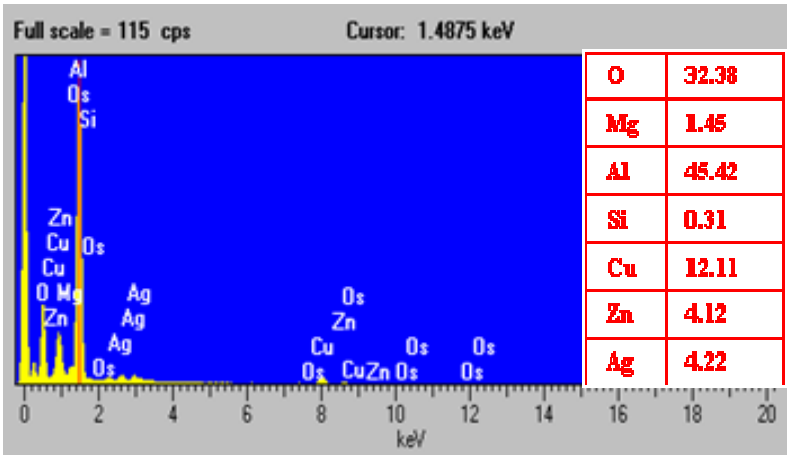

Figure 31. EDS analysis of point 4 for 3 shot.

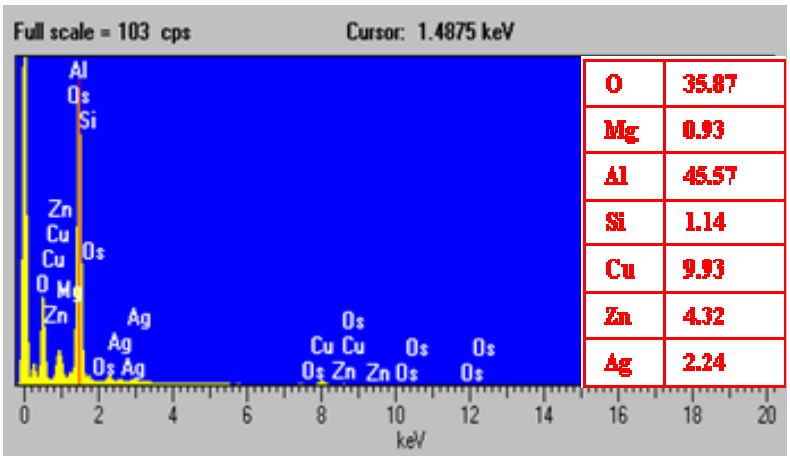

Figure 32. EDS analysis of point 5 for 3 shot.

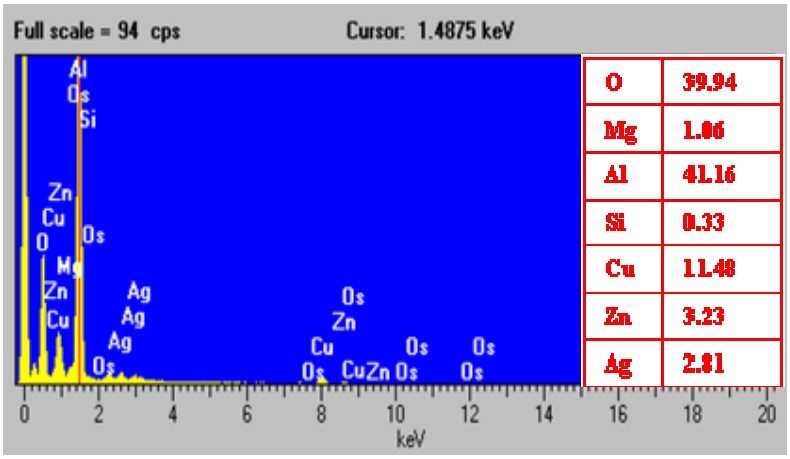

Figure 33. EDS analysis of point 6 for 3 shot.

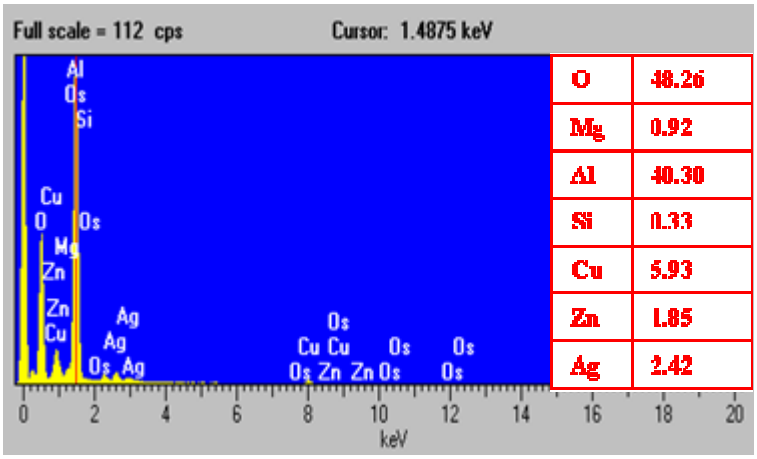

Figure 34. EDS analysis of point 7 for 3 shot.

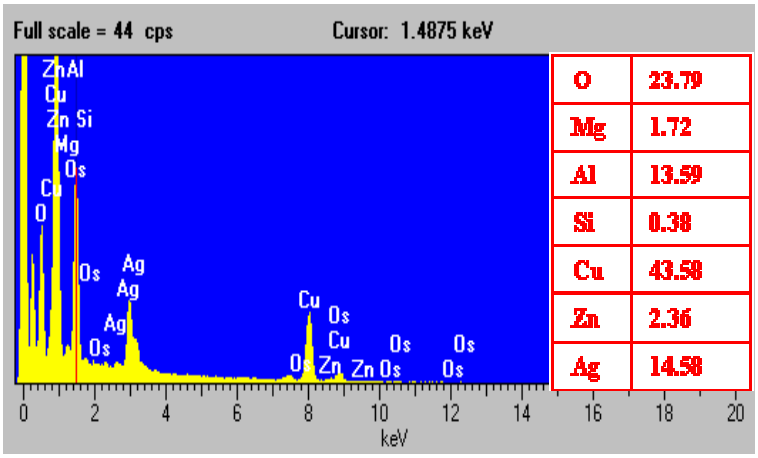

Figure 35. EDS analysis of point 8 for 3 shot.

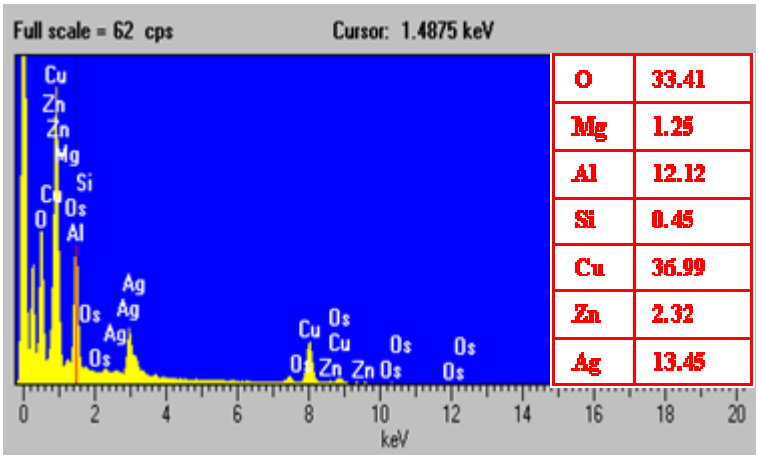

Figure 36. EDS analysis of point 9 for 3 shot.

The combined element concentration graph, shown in Figure 37, for 3 shots was analyzed. At point 1, 15μm below the surface of the rail, expected elemental concentration levels for Cu and Ag were observed. At point 2, the Cu level dropped as expected, but the Ag level increased 4%. This is believed to be caused by outward diffusion of Cu into the Al-rich debris. The diffusive interaction would explain the uneven rail/debris interface. The Cu concentration from points 1-2 has a steeper slope than the one shot graph in Figure 26. Cu diffusing into the debris would leave Ag behind on the rail giving the appearance increased Ag, when in fact, it did not change at all. From points 2-9, Al and O concentrations increase. At points 4-5, the Al concentration is higher than the O concentration, suggesting that the Al is not completely oxidized to Al_20_3. In all likelihood, the debris layer between points 4 and 7 comprises a mixture of oxides and metallic Al. Surprisingly, the concentration of Cu on the top surface layer is high, although the reason for this is unclear at present.

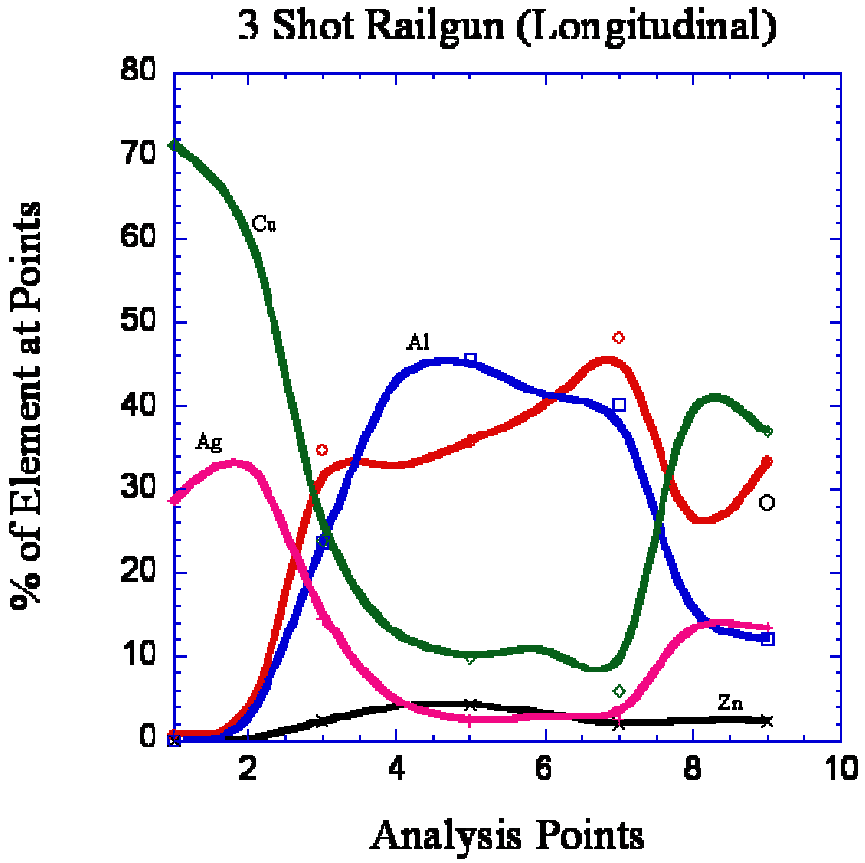

Figure 37. Combined element concentration graph for 3 shot.

3. Rail Cross-Section after 8 Shots

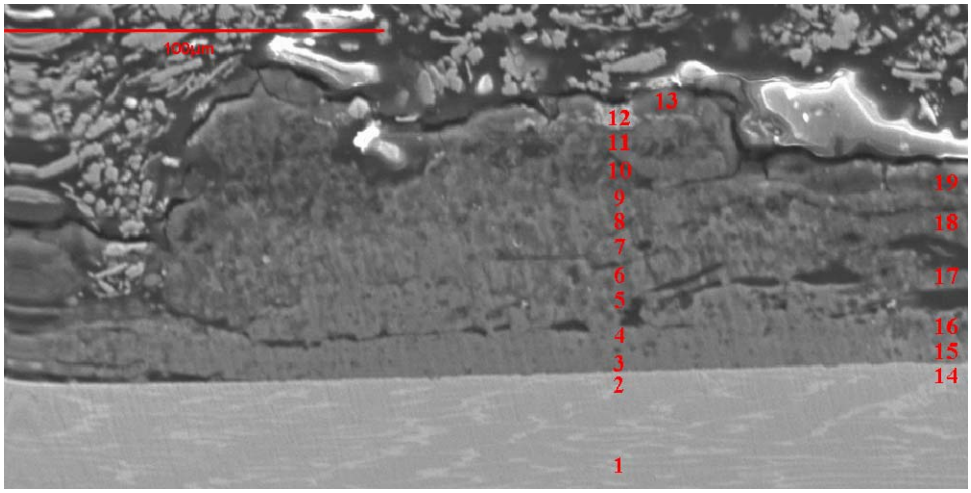

(a) SEM picture of cross-section of rail for 8 shots showing EDS analysis points

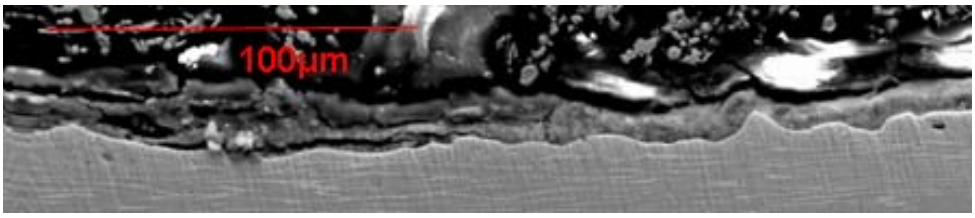

(b) SEM picture of rail for 8 shots showing rail damage

Figure 38. SEM Pictures of 8 shot.

There were several layers present after 8 shots. The rail appeared to be badly damaged with a majority of the rail surface becoming uneven. There were sections of the rail where Al appeared to have corroded into the rail instead of being deposited on the surface of the rail. The debris layer measured 125µm in thickness. This was much thicker than 1 or 3 shot layers. Rail damage was measured 450µm in length and 15µm in depth. This damage was found throughout the rail. Areas of the rail where debris layers were extremely thick underwent very little rail damage, as seen in Figure 38a. Areas where debris thickness was minimal showed extensive rail damage as shown in Figure 38b. This was caused by diffusive interaction between rail and debris followed by the gouging of the debris by the front of the moving armature, which also rips away chunks

of rail with it. Figures 39-51 and Figures 53-58 show the EDS graphs and compositional charges at various points shown in Figure 38a, whereas Figure 52 shows the elemental compositional profiles across the debris.

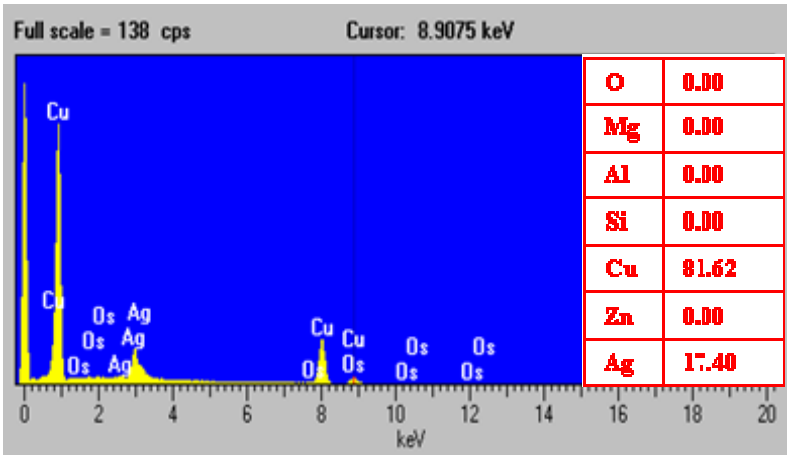

Figure 39. EDS analysis of point 1 for 8 shot.

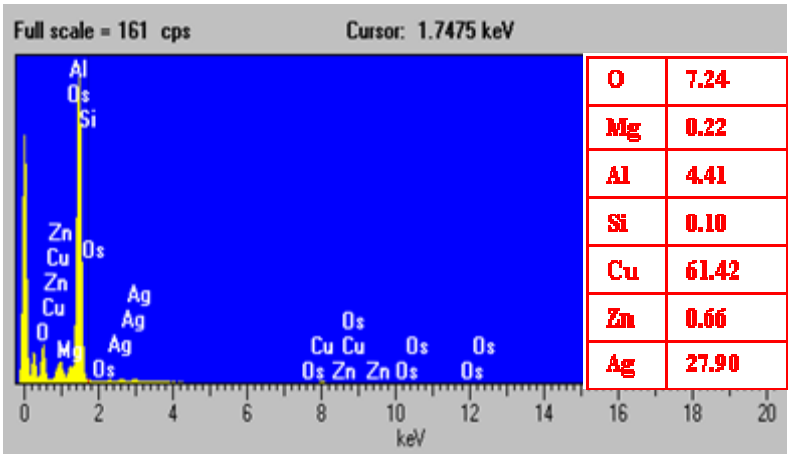

Figure 40. EDS analysis of point 2 for 8 shot.

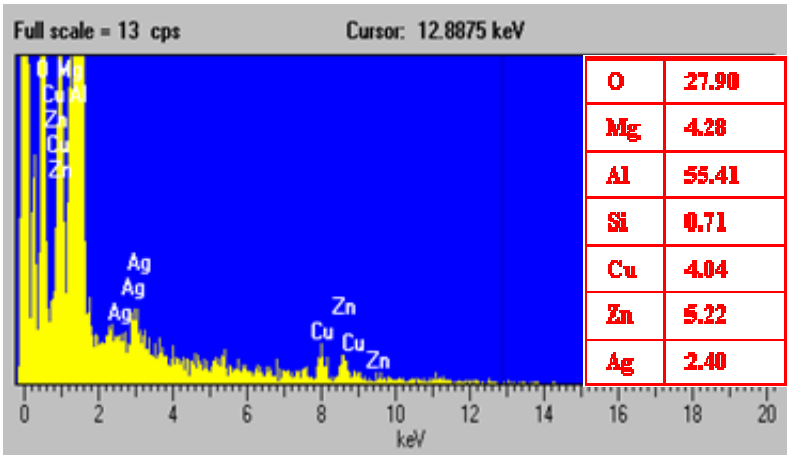

Figure 41. EDS analysis of point 3 for 8 shot.

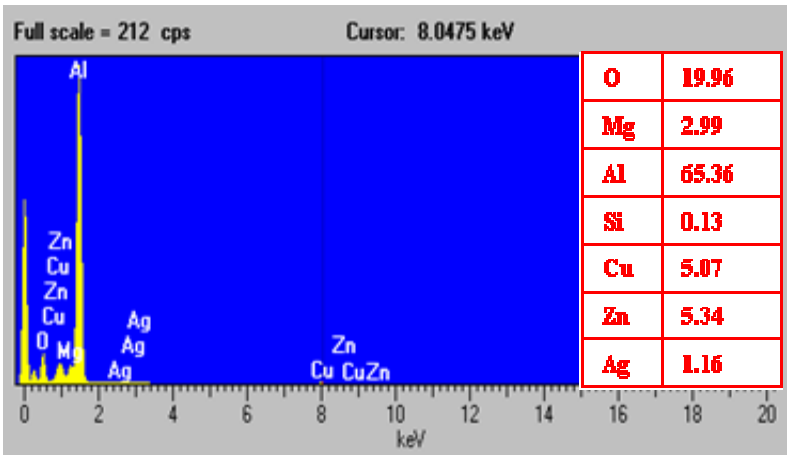

Figure 42. EDS analysis of point 4 for 8 shot.

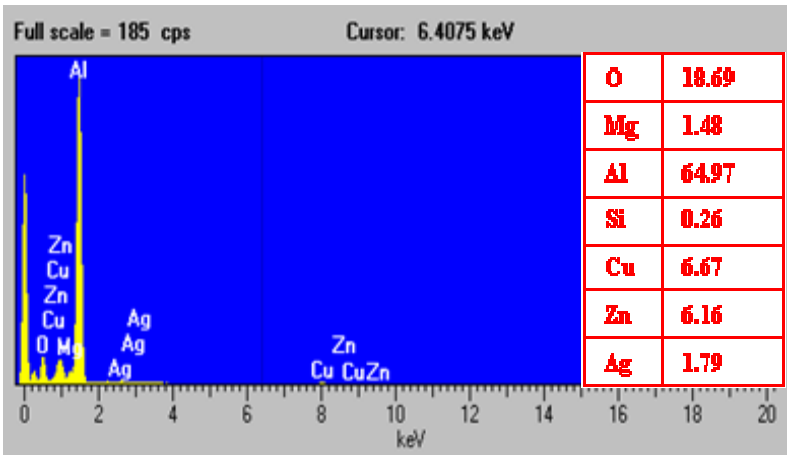

Figure 43. EDS analysis of point 5 for 8 shot.

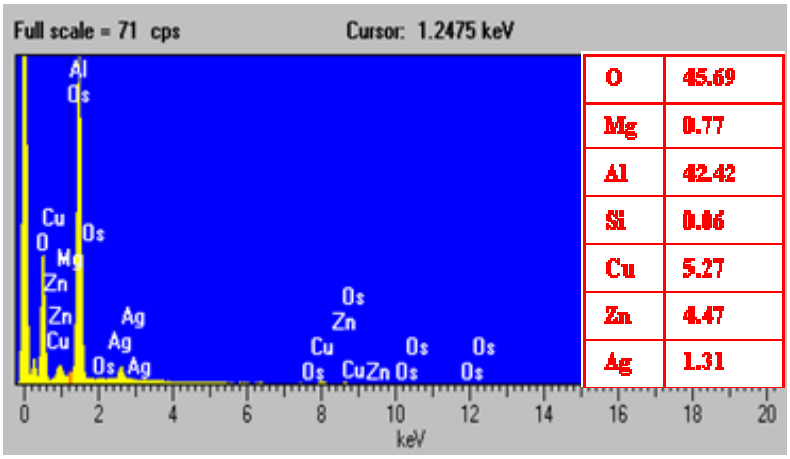

Figure 44. EDS analysis of point 6 for 8 shot.

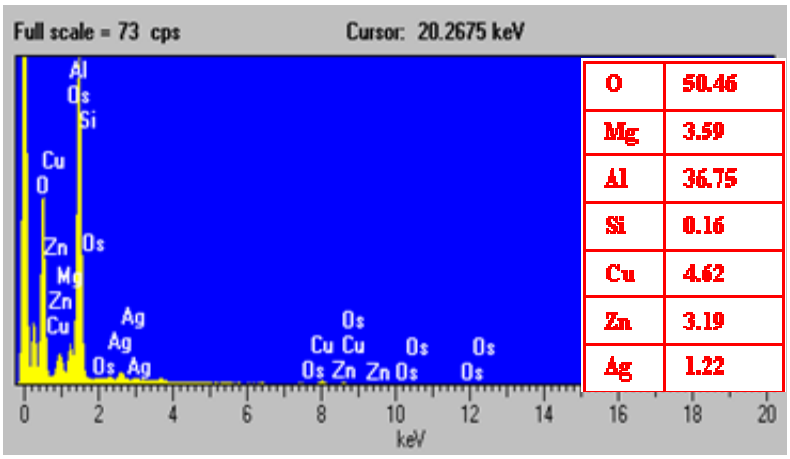

Figure 45. EDS analysis of point 7 for 8 shot.

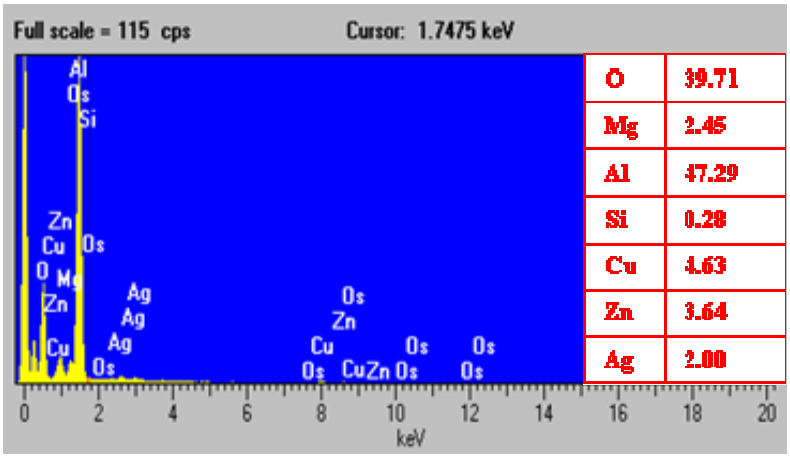

Figure 46. EDS analysis of point 8 for 8 shot.

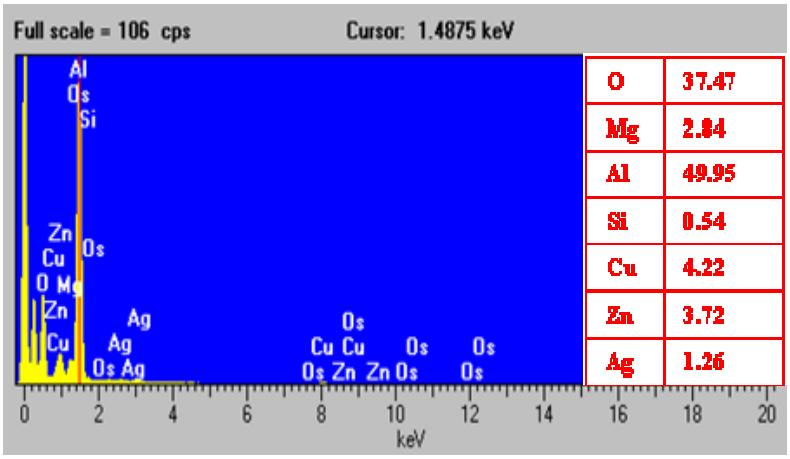

Figure 47. EDS analysis of point 9 for 8 shot.

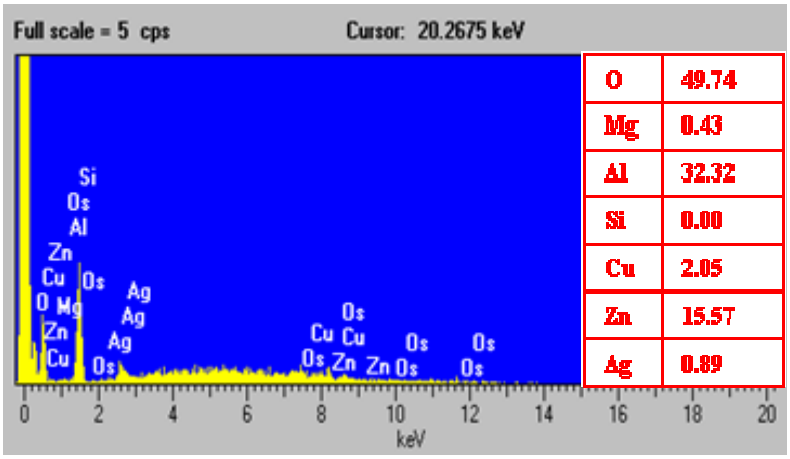

Figure 48. EDS analysis of point 10 for 8 shot.

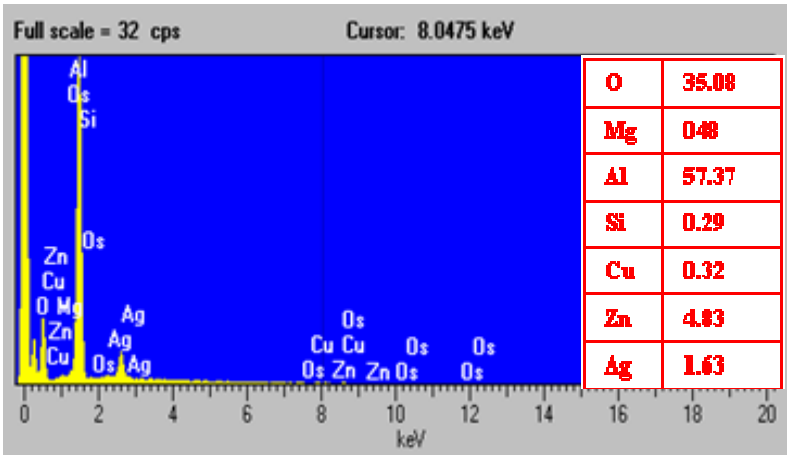

Figure 49. EDS analysis of point 11 for 8 shot.

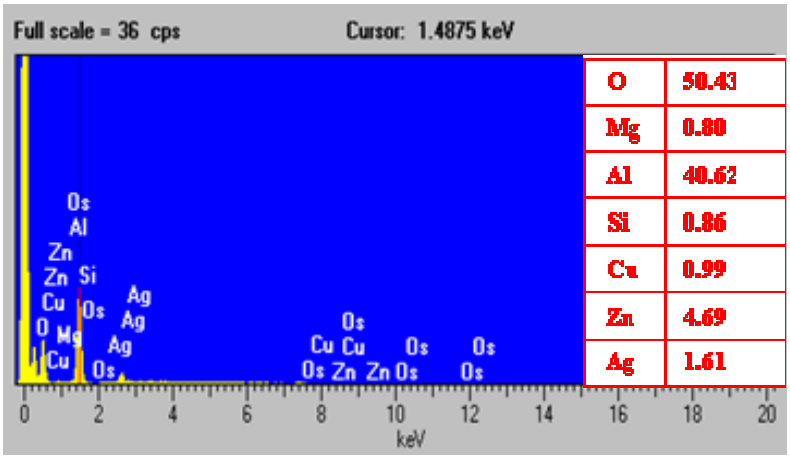

Figure 50. EDS analysis of point 12 for 8 shot.

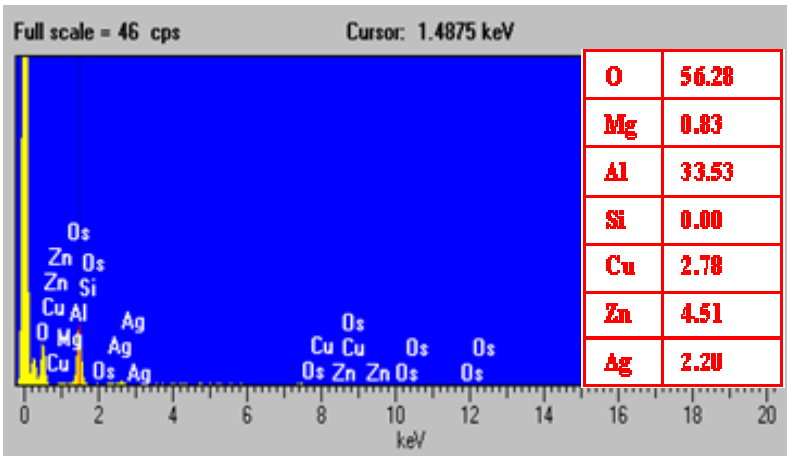

Figure 51. EDS analysis of point 13 for 8 shot.

EDS was completed on the 8 shot rail. Points 1 - 4 show the same behavior as before the in 3 shot measurement. Points 5 – 13 show Cu and Ag continually decreasing while Al and O oscillate between each other throughout the rest of the debris layer. The oscillation is probably due to oxygen concentration differences within each deposited layer with the surface of the various layers being more heavily oxidized.

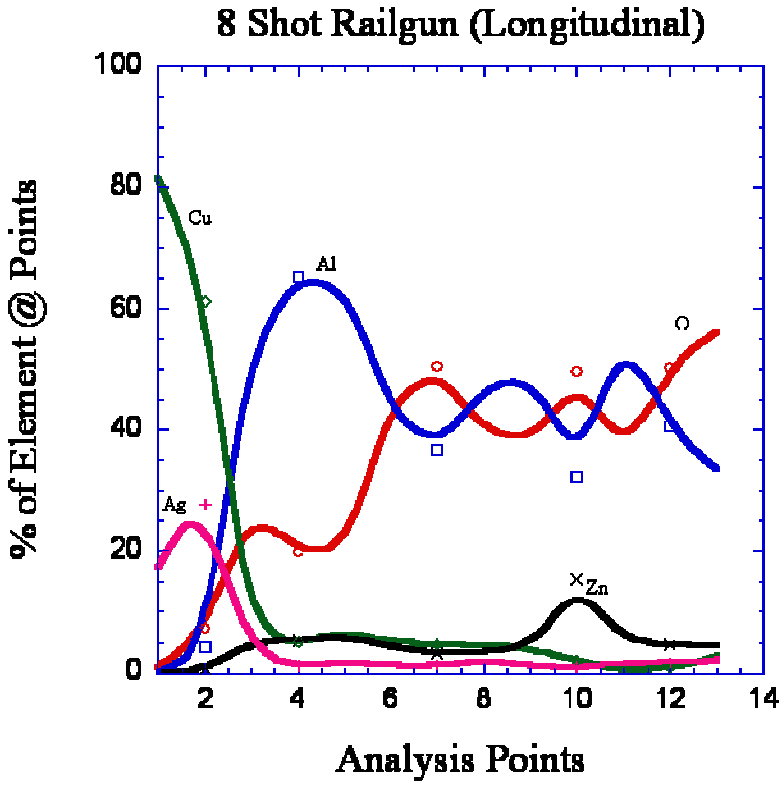

Figure 52. Combined element concentration graph for 8 shot.

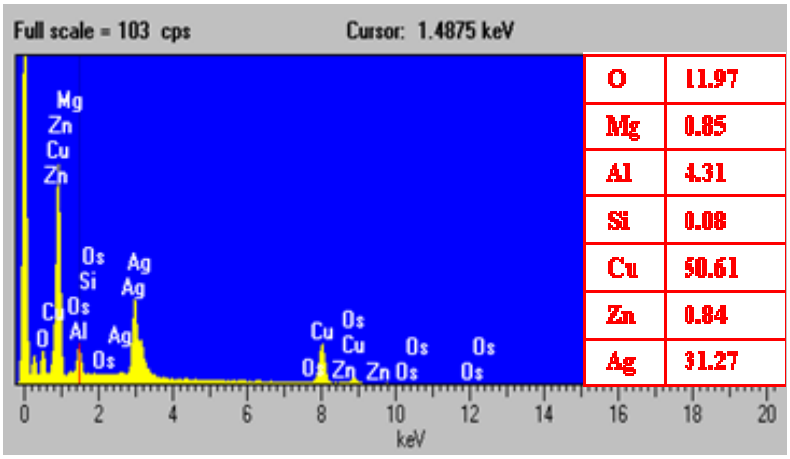

Figure 53. EDS analysis of point 14 for 8 shot.

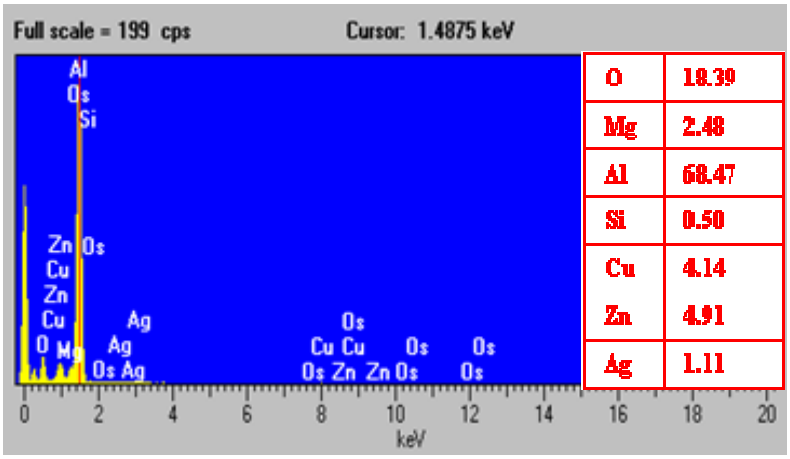

Figure 54. EDS analysis of point 15 for 8 shot.

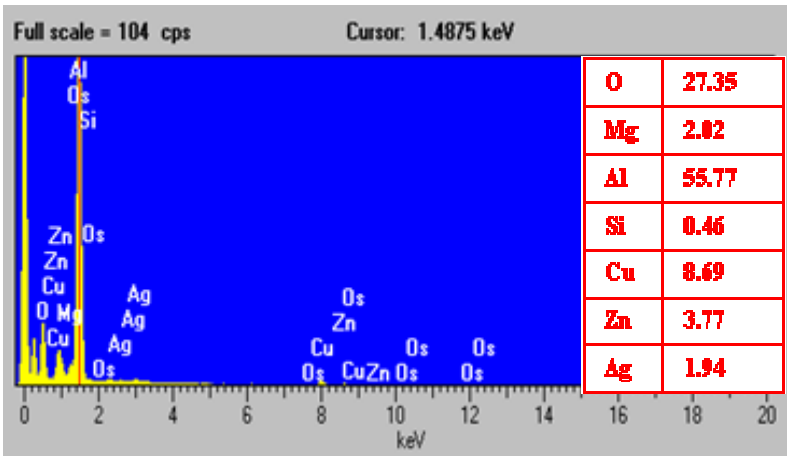

Figure 55. EDS analysis of point 16 for 8 shot.

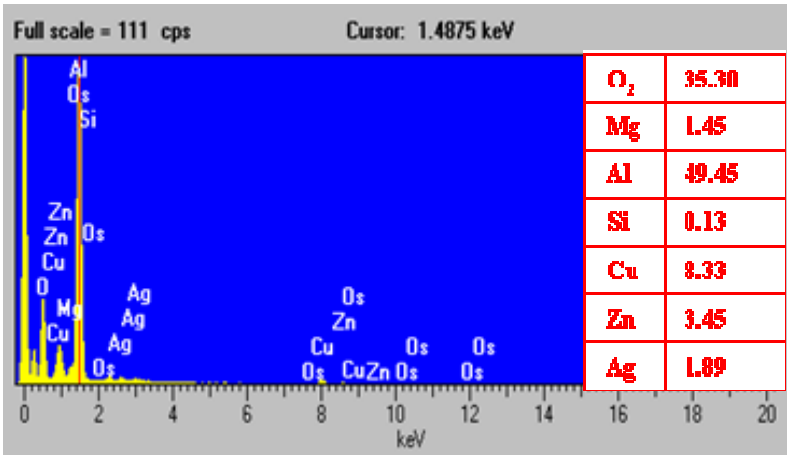

Figure 56. EDS analysis of point 17 for 8 shot.

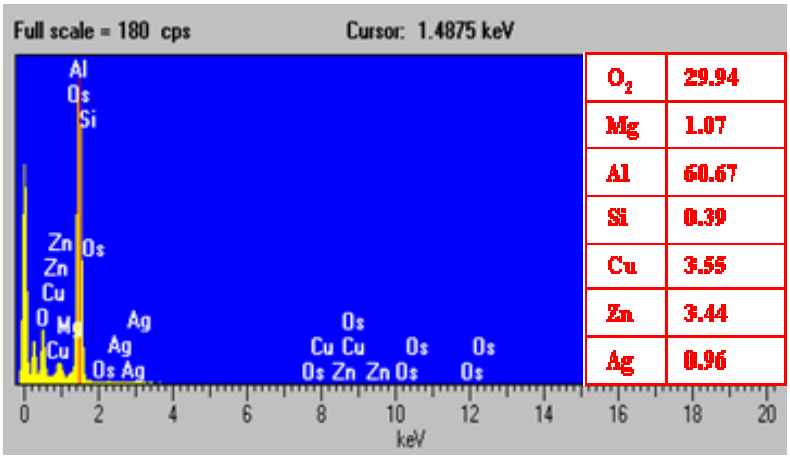

Figure 57. EDS analysis of point 18 for 8 shot.

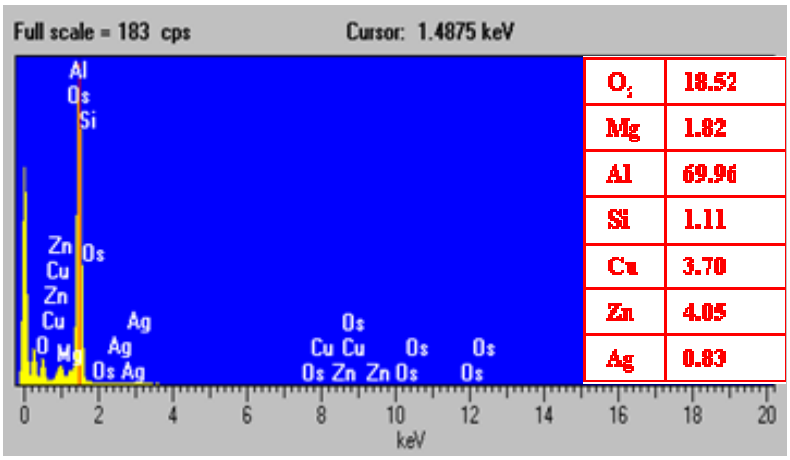

Figure 58. EDS analysis of point 19 for 8 shot.

EDS analysis of a different region (points 14-19, see figure 38a) showed a slightly different behavior than points 1-13 for the same sample. Points 14 and 15 show Al and O with similar results as before, but Cu and Ag did not show an increase in this area. Points 16 – 18 show an increase in Cu, by about 4%, which is not seen in the same sample analyzed at a different location. This rise in the level of Cu is similar to that observed for the sample after 3 shots, as seen in Figure 37. It should be noted that in Figure 37, the elevated Cu concentration is observed at a distance of approximately 20μm for the Cu/debris interface, which is roughly the same distance at which the elevated level of Cu is observed in Figure 59. The rationale for this elevated level of Cu needs further investigation.

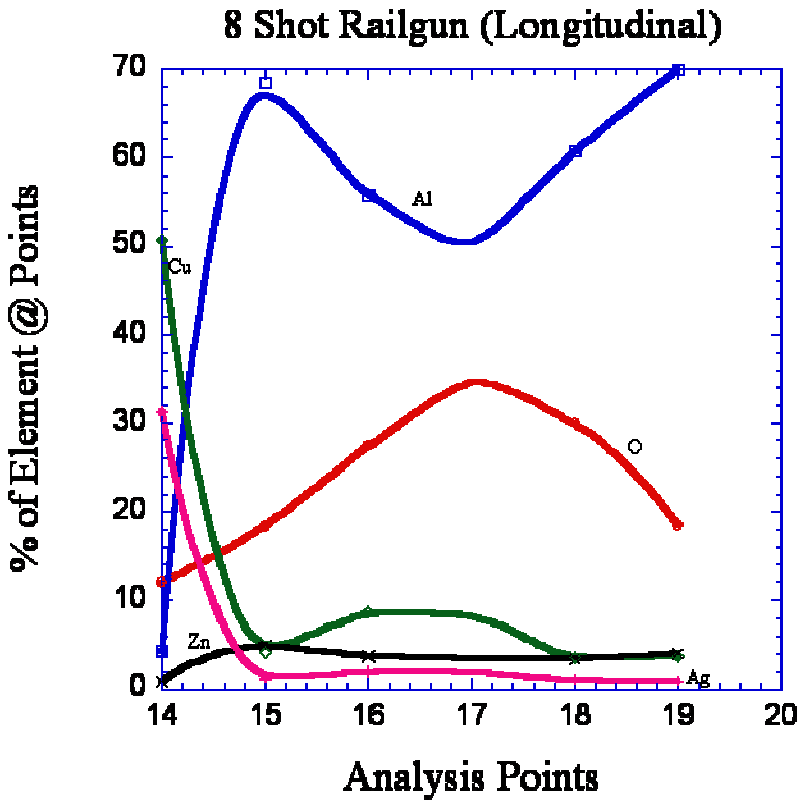

Figure 59. Combined element concentration graph for 8 shot.

VI. CONCLUSIONS AND RECOMMENDATIONS

An earlier study [15] had noted that upon application of a large current density to a Cu thin film line in contact with Al, the Al melts due to Joule heating, and migrates towards the cathode (negative terminal). As a follow-up of ref. [15], the present work utilizes a model system comprising a bead of Ga on a thin film Cu track to study the migration of liquid Ga along the track under the influence of an electric current in an Argon atmosphere. The melt-front velocity was measured in situ as a function of current and temperature using electrical circuitry. It was noted that depending on the applied current and the instantaneous temperature, the Ga-melt front velocity ranged between 10μm/s to 35μm/s. It was further noted that even when the thermal gradient on both sides of a Ga bead was identical, the liquid Ga always migrated in the direction of current flow (i.e., towards the cathode). This observation suggests that electromigration, not thermo-migration, is the principal driving force for the observed migration. From the measured velocities, the activation energy for migration was computed to be 17.35kJ/mole, which was close to the activation energy for Ga self diffusion in the liquid state. It is therefore concluded that the Ga melt migrates via electromigration of Ga in the liquid under the influence of the direct electrostatic force.

The debris deposited on Cu/24Ag rails following firing of 7075Al armatures in an electromagnetic railgun was also studied. Previous work had noted that the source of the deposit can be due to interfacial tribological effects, as well as due to local melting of the Al armature due to electric current crowding [33]. In this study, the compositional variation across the cross-section of the deposit was analyzed. The deposit was found to be principally aluminum with a significant amount of oxygen, suggesting that the molten Al deposited on the rail during firing of a railgun is in a partially or completely oxidized state. Substantial porosity was also observed within the deposit, possibly due to hydrolysis of molten Al, in accordance with the observations of references [13 and 14].

Future study should be undertaken to determine the kinetics of 7075Al using the procedures performed in this thesis. The kinetics of 7075Al could then be scaled to current railgun prototypes to model the potential damage and effect electromigration can cause when firing railguns. The kinetics of 7075Al along with the compositional evolution of rail debris will aid in solving current railgun problems.

LIST OF REFERENCES

1. McNab, I.R. "Early Electric Gun Research." IEEE Transactions of Magnetics 35.1 (1999) 250-261.

2. Luke, I.T., M.F. Stumborg. "The Operational Value of Long Range Land Attack EM Guns to Future Naval Forces." IEEE Transactions of Magnetics 37.1 (2001) 58-61.

3. McNab, I.R., F. Stefani, M. Crawford, M. Erengil, C. Persad, S. Satapathy, H. Vanicek, T. Watt, C. Dampier. "Development of a Naval Railgun." IEEE Transactions of Magnetics 41.1 (2005) 206-210.

4. Barber, J.P., D.P. Bauer, K. Jamison, J.V. Parker, F. Stefani, and A Zielinski. A Survey of Armature Transition Mechanisms." IEEE Transactions of Magnetics 39.1 (2003) 47-51.

5. Barber, J.P., I.R. McNab. "Magnetic Blow-off in Armature Transition." IEEE Transactions of Magnetics 39.1 (2003) 42-46.

6. DeGaspari, J. "Extreme Tribology." ASME Mechanical Engineering Magazine 126.9 (2004) 10-11.

7. Price, J.H., C.W.G. Fulcher, M.W. Ingram, D.E. Perkins, D.R. Peterson, R.C. Zowarka, J.A. Pappas. "Design and Testing of Solid Armatures for Large-bore Railguns." IEEE Transactions of Magnetics 25 (1989) 467-473.

8. Karthaus, W., W.A. de Zeeuw, W.J. Kolkert. "On the Design and Testing of Solid Armatures for Rail Accelerator Applications." IEEE Transactions of Magnetics 27 (1991) 308-313.

9. Persad, C., A. Yeoh, G. Prabhu, G. White, Z. Eliezer. "On the Nature of the Armature-Rail Interface: Liquid Metal Effects. IEEE Transactions of Magnetics 33 (1997) 140-145.

10. Kerwien, S.C. "Metallurgical Analysis of an Aluminum Sabot Fired in the Cannon Caliber Electromagnetic Gun (CCEMG)." IEEE Transactions of Magnetics 33 (1997) 104-108.

11. Stefani, F., J.V. Parker. "Experiments to Measure Wear in Aluminum Armatures [in railguns]. IEEE Transactions of Magnetics 35 (1999) 100-106.

12. Meger, R.A., K. Cooper, H. Jons, J. Neri, S. Qadri, I.L. Singer, J. Sprague, K.J. Wahl. "Analysis of Rail Surfaces from a Multishot Railgun." IEEE Transactions of Magnetics 41 (2005) 211-213.

13. Persad, C., Z. Castro. "Railgun Tribology: Characterization and Control of Multishot Wear Debris." IEEE Transactions of Magnetics, in press, (2007).

14. Persad, C. "Railgun Tribology: Chemical Reactions between Contacts." IEEE Transactions of Magnetics, in press, (2007).

15. Delaney, L. "A First Report on Electromigration Studies at a Model Cu-Al Railgun Contact." Thesis, Naval Postgraduate School (2006).

16. Ho, P. S., T. Kwok. "Electromigration in Metals." Reports on the Progress in Physics 52 (1989) 301-348.

17. Blech, I. A. "Electromigration and crevice formation in thin metallic films." Thin Film Solids 13 (1972) 117-129.

18. Blech, I. A., E. Kinsbron. "Electromigration in Thin Gold Films on Molybdenum Surfaces." Thin Solid Films 25 (1975) 327-334.

19. Blech, I. A. "Electromigration in thin aluminum films on titanium nitride." Journal of Applied Physics 47 (1976) 1203-1208.

20. Blech, I. A., C. Herring. "Stress generation by electromigration." Applied Physics Letters 29.3 (1976) 131-133.

21. Black, J. R. "Electromigration- A Brief Survey and Some Recent Results." IEEE Transactions on Electron Devices 16.4 (1969) 338-347.

22. Yasunaga, H., A Natori. "Electromigration on semiconductor surfaces." Surface Science Reports 15 (1992) 205-280.

23. Lodder, A. "Clarification of the Direct-Force Controversy in Electromigration Theory." Solid State Communications 79.2 (1991) 143-146.

24. Kono, S., T. Goto, Y. Ogura, T. Abukawa, "Surface electromigration of metals on Si(001): In/Si(001)." Surface Science 420 (1999) 200-212.

25. Dekker, J. P., A. Lodder. "Theory for the electromigration wind force in dilute alloys." Physical Review B 56.19 (1997) 167-177.

26. Anthony, T. R. "The electromigration of liquid metal inclusions in Si." Journal of Applied Physics 51 (1980) 6356-6365.

27. Epstein, S. G., A. Paskin. "Atom Motion in Liquid Alloys in the Presence of an Electric Field." Physics Letters 24A.6 (1967) 309-310.

28. Regan, B. C., S. Aloni, R. O. Ritchie, U. Dahmen, A. Zetti. "Carbon nanotubes as nanoscale mass conveyors." Nature 428.6986 (2004).

29. Lee, P.D., J. Hunt, "Hydrogen porosity in directional solidified aluminum alloys: in situ observation." Acta Materialia 45.10 (1997) 4155-4169.

30. Samuel A.M., F.H. Samuel. "Various aspects involved in the production of low-hydrogen aluminum castings-Review." Journal of Materials Science 27.24 (1992) 6533-6563.

31. Talbot, D. "The effects of hydrogen in aluminum and its alloys." London: Maney Publishing, on behalf of the Institute of Materials, Minerals and Mining. (2004).

32. Brandes, E.A., G. Brook. "Self Diffusion in Liquid Metal, Table 13.6." Smithells Metals Reference Book. 7th Ed. 118.

33. Chen, T., X. Long, I. Dutta, C. Persad. "Effects of Current Crowding on Microstructural Evolution at Rail-Armature Contacts in Railguns." IEEE Transactions of Magnetics, in review, (2006).

34. Wikipedia website, last accessed on 9 November 2006 http:/en.wikipedia.org/wiki/electromigration

THIS PAGE INTENTIONALLY LEFT BLANK

INITIAL DISTRIBUTION LIST

1. Defense Technical Information Center
   Ft. Belvoir, Virginia

2. Dudley Knox Library
   Naval Postgraduate School
   Monterey, California